Carbohydrate Polymers 378 (2026) 124919

Contents lists available at ScienceDirect

Carbohydrate Polymers

journal homepage: www.elsevier.com/locate/carbpol

Biochemical characterisation of the 4-α-glucanotransferase from the hyperthermophilic archaeon *Pyrobaculum arsenaticum* and its formation of high-amylose resistant starch

Oriana Sacco [a,b], Emilie Louise Johansen [c], Yu Tian [d], Jesper Holck [e], Jacob Judas Kain Kirkensgaard [f,g], Andreas Blennow [h,1], Federica De Lise [a], Ali Shaikh-Ibrahim [a], Marco Moracci [b,i], Nicola Curci [a,*], Birte Svensson [j,*], Beatrice Cobucci-Ponzano [a,*], Yu Wang [j,k,**]

[a] *Institute of Biosciences and BioResources, National Research Council of Italy, via P. Castellino, 111, 80131, Naples, Italy*
[b] *Department of Biology, University of Naples Federico II, Via V.C. Cintia, 26, 80126, Napoli, Italy*
[c] *Department of Plant and Environmental Sciences, University of Copenhagen, DK-1871, Frederiksberg C, Denmark*
[d] *Lab of Food Soft Matter Structure and Advanced Manufacturing, College of Food Science and Engineering, Collaborative Innovation Center for Modern Grain Circulation and Safety, Nanjing University of Finance and Economics, Nanjing, 210023, China*
[e] *Protein Chemistry and Enzyme Technology Section, DTU Bioengineering, Department of Biotechnology and Biomedicine, Technical University of Denmark, Lyngby, Denmark*
[f] *Department of Food Science, University of Copenhagen, DK-1958, Frederiksberg C, Denmark*
[g] *Niels Bohr Institute, University of Copenhagen, DK-2100, Copenhagen Ø, Denmark*
[h] *Blennow Holding AB, SE-217 52, Malmö, Sweden*
[i] *NBFC, National Biodiversity Future Center, Palermo, Italy*
[j] *Enzyme and Protein Chemistry, Department of Biotechnology and Biomedicine, Technical University of Denmark, DK-2800, Kgs. Lyngby, Denmark*
[k] *Department of Food Nutrition and Safety/National R&D Center for Chinese Herbal Medicine Processing, College of Engineering, China Pharmaceutical University, Nanjing, 211198, China*

ARTICLE INFO

Keywords:
High-amylose starch granules
Hyperthermophile 4-α-glucanotransferase
Starch structure
Resistant starch
Starch *in vitro* digestion
Interfacial kinetics

ABSTRACT

High-amylose starch (HAS) is gaining attention in biotechnology for its thermal stability, structural resilience and health benefits. Its dense crystalline structure hinders hydrolysis by human gut enzymes, making it a promising source of type 2 resistant starch for hydro-thermal and enzymatic upgrading. 4-α-Glucanotransferases (4αGTs) of glycoside hydrolase family 77 catalyse disproportionation of α-1,4-glucan chains in HAS, enhancing functionality and nutritional properties. Here, a 4αGT, *Par*GT from the hyperthermophilic archaeon *Pyrobaculum arsenaticum,* identified in a metagenomic dataset from Pisciarelli hot spring (85 °C, pH 5.5; Naples, Italy), showed highest activity at 100 °C and pH 5.5, and specific activity of maltotriose disproportionation at 75 °C of 1170 U/mg. *Par*GT effectively modified HAS granules under controlled heating (annealing) at 75 °C, altering crystallinity, surface order and chain length. Comparative analysis of native, heat-treated and *Par*GT-modified HAS granules from wheat, potato, maize, and barley revealed distinct effects of botanical source, enzymatic modification, and heating. Notably, *Par*GT increased the resistant starch (RS) contents in wheat and potato HASs subjected to *in vitro* digestion. Interfacial kinetics correlated the increased resistance to decreased density of glucoamylase attack sites. Overall, *Par*GT showed strong potential in enzyme- and hydro-thermal modifications developing starch-based ingredients for health and food applications.

* Corresponding authors.
** Correspondence to: Y. Wang, Enzyme and Protein Chemistry, Department of Biotechnology and Biomedicine, Technical University of Denmark, DK-2800, Kgs. Lyngby, Denmark.
E-mail addresses: nicola.curci@cnr.it (N. Curci), bis@bio.dtu.dk (B. Svensson), beatrice.cobucciponzano@cnr.it (B. Cobucci-Ponzano), yuwang@cpu.edu.cn (Y. Wang).
[1] Department of Biotechnology and Food Engineering, Guangdong Technion-Israel Institute of Technology, Shantou, 515063, China.

https://doi.org/10.1016/j.carbpol.2026.124919
Received 9 October 2025; Received in revised form 7 January 2026; Accepted 11 January 2026
Available online 12 January 2026

1. Introduction

Starch is a major carbohydrate reserve in plants and a key component in human diets and industrial food formulations (Baghurst et al., 1996; Dobranowski & Stintzi, 2021; Smith & Zeeman, 2020). Starch is deposited as semi-crystalline granules composed of two α-glucans, namely the essentially linear α-1,4-linked amylose and the branched amylopectin containing about 5% α-1,6-linkages. The amylose/amylopectin ratio varies among different starch types and influences their structural, functional, and nutritional properties (Smith & Zeeman, 2020). High-amylose starch (HAS) gained interest due to its reduced digestibility, being a promising source of resistant starch (RS) that is less susceptible to enzymatic degradation in the gastrointestinal tract and considered a dietary fibre (Tian et al., 2023; Tian et al., 2025). HASs are classified as RS type 2 (RS2), resisting digestion due to the compact molecular organisation and associated with several health benefits, including reduced glycaemic response, optimal gut microbiota composition, reduced risk of metabolic disorders such as type 2 diabetes and obesity, and immunomodulatory effects (Chuang et al., 2012; Gidley, 2013; Yin et al., 2023). HAS thus acquired prominence in food, pharmaceutical and biomaterials applications like for RS-enriched formulations, controlled drug delivery systems, and biodegradable packaging materials (Li et al., 2019; Liu et al., 2022; Zhu, 2017). Notably, HASs exhibit higher gelatinization temperatures than normal starches having lower amylose content (Jayakody & Hoover, 2008; Tian, Liu, et al., 2024), largely attributed to compact crystallinity and other organizational features of the HAS granules. This structural resilience plays a key role in preserving starch architecture and promoting the retention of RS in final products. To modulate the HAS structure, hydrothermal treatment and annealing, are used to induce rearrangement of the α-glucan molecules at high temperature, resulting in increased RS content. In annealing, controlled hydration and heating to a temperature slightly above the onset of gelatinization promote molecular mobility in amorphous and crystalline regions without starting gelatinization, thus retaining granular integrity (Fonseca et al., 2021; Li et al., 2020). In addition to physical treatments, chemical modifications, including acid hydrolysis, oxidation, or crosslinking with phosphates, have been used to alter starch properties (Ayoub & Rizvi, 2009; Pandiselvam et al., 2019; Wang & Copeland, 2015). These methods can introduce new functional groups or partially depolymerise starch, but often require harsh reagents, extreme pH, or high temperatures, which may degrade the starch or generate undesirable by-products. Compared with chemical treatments, hydrothermal approaches like annealing are milder, preserve granular integrity, and maintain the natural crystalline structure of high-amylose starch, though the extent of modification is more limited and may require optimization of temperature, hydration, and treatment duration (Compart et al., 2023).

In addition to thermal treatment, enzymatic modification presents a mild and useful approach for tailoring properties of granular starch. 4-α-Glucanotransferases (4αGTs, EC 2.4.1.25), are among the preferred carbohydrate active enzymes (CAZymes) for starch modification (Chen et al., 2023; Christensen et al., 2024; Nakapong et al., 2022; Punia Bangar et al., 2022). 4αGTs, also known as disproportionating enzymes (D-enzyme) in plants and as amylomaltases in bacteria and archaea, are found in glycoside hydrolase (GH) families 13, 57, and 77 of the CAZy database (www.cazy.org; Drula et al., 2022). Notably, family GH77 is monospecific and contains only 4αGTs. 4αGTs act with remarkable versatility in disproportionation, coupling, cyclization and hydrolysis reactions through a double-displacement (anomer retaining) mechanism. In this process, the enzyme first cleaves an α-1,4-glucosidic bond in an α-1,4-D-glucan (donor) with formation of a covalent glucanosyl–enzyme intermediate, that transfers the glucan fragment to an acceptor molecule (Lombard et al., 2025). Depending on the acceptor being either water, or O4 of the non-reducing end residue of the internal glucan, or of another glucan chain, the enzyme can release glucose/short oligosaccharides (hydrolysis), generate cyclic glucans (cyclization), elongate and shorten chains (disproportionation) or join two α-glucan chains (coupling) (Chen et al., 2023; Kim et al., 2021; Wang, Tian, Møller, et al., 2025). Previous studies have explored the modification of gelatinised starch at high temperature as well as granular starch at lower temperature using 4αGT from *Thermoproteus uzoniensis*. These modifications, which led to change in chain length distribution, degree of granular surface order and crystallinity, included interfacial kinetic analysis quantifying enzymatic attack sites on the granular surface (Wang et al., 2020; Wang, Tian, Rennison, et al., 2025). Building on this foundation, we hypothesize that HAS granules modified by thermostable enzymes at high temperature, but without inducing gelatinisation, retain granular features while undergoing targeted structural and functional changes. This approach may enable the development of tailored modified starches for nutritional and biotechnological applications, including functional foods, biomaterials, and advanced delivery systems (Leoni et al., 2021). Moreover, such elevated-temperature conditions for HAS modification may also improve process robustness and make the approach more suitable for the food industry.

The CAZy database lists more than 21,000 sequences in family GH77 (www.cazy.org/GH77), but only 27 4αGTs, including 9 from thermophiles, have been characterised. Thermostable enzymes pose a general priority for industrial processes due to their robustness under harsh conditions (Curci et al., 2021; De Lise et al., 2023; Shaikh-Ibrahim et al., 2025) and appear particularly well-suited for modification of HAS granules, having high gelatinization temperatures. Here, *Pyrobaculum arsenaticum Par*GT (Jung et al., 2025), whose gene was identified in a metagenomic dataset derived from an 85 °C, pH 5.5 solfataric mud pool in the Pisciarelli hot spring, Agnano (Naples, Italy) (Strazzulli et al., 2020), was used to modify granular HASs under annealing-like conditions. By comparing both thermally- and *Par*GT-modified with native and only thermally-treated HAS granules from four different botanical sources, roles were outlined of molecular rearrangements shaping structural and physicochemical properties of tailored starch granules. Therefore, this study aimed to provide the first systematic analysis of HAS granule modification using a hyperthermophilic 4αGT under high-temperature, non-gelatinising conditions. This included thorough investigation of several conditions to capture factors contributing to granular starch modification, also evaluating resistant starch (RS) content, revealing a complex interplay of structural modification and altered functional behaviour achieved by thermophilic 4αGT and thermal treatments.

In vitro digestion of modified HAS granules using pancreatin and glucoamylase (Englyst et al., 1992), together with glucoamylase interfacial kinetic studies, provided insights on the impact of the molecular rearrangements behind formation of RS. Collectively, our findings led to new understanding of thermophilic 4αGTs harnessed to tailor functional starch-based materials for nutritional food and industrial applications (Arruda et al., 2025; Reddy Shetty et al., 2021).

2. Material and methods

2.1. Materials

Maltooligosaccharides (MOS) of degree of polymerization (DP) 3–7 (G3-G7) and *Bacillus licheniformis* pullulanase M2 were from Megazyme (Bray, Ireland). Amylose type III from potato, *Aspergillus niger* glucoamylase (GA) and pancreatin, containing porcine pancreatic α-amylase (PPA), were from Sigma-Aldrich (St. Louis, MO). *E. coli* Lemo21 (DE3) was used as host for heterologous recombinant *Par*GT production and the plasmid containing the *parGT* gene was previously described (Strazzulli et al., 2020). High-amylose/high-phosphate potato starch (HPPS) (Blennow et al., 2005) and amylose-only barley starch (AOB) (Carciofi et al., 2012) were obtained as described. High-amylose maize starch (AE), and high-amylose wheat starch (HAWS) were acquired from experimental fields of Northwest A&F University, Yangling, China. HAS amylose contents and abbreviated names are given in Table 1. All

Table 1
Description of high amylose starch granules.

HAS	Abbreviation	Amylose (%)[1]
Amylose Extender 35 maize starch	AE	72.2
Amylose-Only Barley starch	AOB	99.9
High-amylose/high-Phosphate Potato starch	HPPS	35.2
High-Amylose Wheat Starch	HAWS	67.2

[1] (Tian et al., 2025).

chemicals were of analytical grade.

2.2. Bioinformatic analysis of GH77

The gene *gh77_pool1* encoding *Par*GT was identified in a metagenomic dataset from the Pisciarelli solfatara in Naples (Italy) (Strazzulli et al., 2020). Multiple sequence alignment of *Par*GT with characterised members of family GH77, was constructed and analysed using Clustal W (Thompson et al., 1994) and visualized using ESPript3 (Robert & Gouet, 2014). An AlphaFold 3D predicted structural model of *Par*GT (Abramson et al., 2024), was visualized, analysed, overlayed and compared with crystal structures of 4αGTs of family GH77 using PyMol software (Schrödinger & DeLano, 2020).

2.3. Production and purification of ParGT

The archaeal gene *gh77_pool1* encoding *Par*GT (ABP49821.1) was cloned in the pHTP1 vector with an encoded *N*-terminal His-tag, as described (Strazzulli et al., 2020). *Par*GT was produced recombinantly in Lemo21(DE3) competent *E. coli* cells using Luria-Bertani (LB) media supplemented with 50 μg/mL kanamycin and 20 μg/mL chloramphenicol. Expression was induced at $OD_{600} = 0.6$ by adding 0.1 mM isopropyl-β-D-thiogalactopyranoside (IPTG) and the culture was grown at 20 °C for 18 h under shaking. Cells were harvested by centrifugation at 3500*g*, resuspended 1:5 (w:v), in 50 mM sodium phosphate, 300 mM NaCl, 5 mM imidazole, pH 8.0 (Buffer A), supplemented with 20 mg lysozyme, 5 mg DNase I, and 1% (*v*/v) Triton X-100, incubated (30 min, RT), and lysed using a multi-cycle high-pressure cell disrupter set to 20 KPSI. The lysate was clarified by centrifugation (16,000 *g*, 30 min, 4 °C) and *Par*GT was purified using the ÄKTA Pure FPLC system (GE Healthcare, IL, USA) equipped with a 1 mL HisTrap™ FF Crude prepacked column (Cytiva, MA, USA), pre-equilibrated with Buffer A. Following an initial wash by 10 column volumes (CV, Buffer A), protein was eluted by a stepwise gradient of 10 CV at 5% and 10 CV at 50% Buffer B (Buffer A supplemented with 500 mM imidazole). Fractions containing 4αGT activity were pooled, concentrated to 5 mL, and further purified by size exclusion chromatography on a HiLoad® 16/600 Superdex® 200 prep grade gel filtration column (GE-Healthcare) pre-equilibrated and eluted by 25 mM HEPES, 100 mM NaCl buffer, pH 7.3, at a flow rate of 1 mL/min. Protein concentration was determined by the Bradford method using bovine serum albumin (BSA) as standard (Bradford, 1976). The native molecular mass of *Par*GT was determined using a Superdex® 200 Increase 10/300 GL column, in the same buffer at a flow rate of 0.5 mL/min and calibrated by ribonuclease A (13.7 kDa), carbonic anhydrase (29.0 kDa), ovalbumin (44.0 kDa), conalbumin (75.0 kDa), aldolase (158 kDa), ferritin (440 kDa), and thyroglobulin (669 kDa). The theoretical monomer molecular mass was calculated using the ExPASy website (Gasteiger et al., 2003) and confirmed by SDS-PAGE.

2.4. Activity assays

2.4.1. Disproportionation standard assay

The standard assay of *Par*GT (12 nM) activity used 40 mM maltotriose (G3) at 75 °C in 100 mM citrate-phosphate pH 5.5 under agitation (500 rpm) for 1 min. The reaction was stopped on dry ice and glucose was quantified using GOPOD D-glucose detection kit reagent (Megazyme, Ireland) and glucose (0.5–5.5 mM) as standard (Huggett & Nixon, 1957). One unit (U) of disproportionation activity was defined as the amount of enzyme releasing 1 μmol/min glucose under the above conditions. Disproportionation activity on 40 mM maltotetraose (G4), maltopentaose (G5), maltohexaose (G6), and maltoheptaose (G7) was determined using the standard assay conditions.

2.4.2. Effects of pH, temperature and metal ions on enzyme activity

pH optimum for *Par*GT was determined on 40 mM G3 in 100 mM sodium-citrate, citrate-phosphate and Tris HCl buffers spanning pH 3.5–8.5. The substrate was pre-incubated (75 °C, 2 min), added enzyme (12 nM final concentration) and after 1 min the reaction was stopped on dry ice. Glucose was quantified as above (see 2.4.1.). Temperature activity dependence was determined at 35–100 °C on G3 in 100 mM citrate-phosphate pH 5.5 as above. The effect on activity of 5, 20 and 40 mM metal ions (K^+, Na^+, Cu^{2+}, Ca^{2+}, Fe^{3+}, Mg^{2+}, Mn^{2+} and Zn^{2+}) was determined under the same conditions as above at 75 °C.

2.4.3. Thermal stability

*Par*GT (120 nM) stored in 25 mM HEPES, 100 mM NaCl, pH 7.3 was incubated at 65, 75, and 85 °C. Aliquots were withdrawn at time intervals and centrifuged (13,000 *g*, 1 min) and the activity (of 12 nM *Par*GT) was determined using the disproportionation standard assay (see 2.4.1.). Activity before the incubation was set to 100%.

2.4.4. Amylose total activity standard assay

Amylose (40 mg/mL) was dissolved in 1 mL 2 M NaOH, diluted 1:1 (v:v) with deionised water, yielding 20 mg/mL amylose in 1 M NaOH, and neutralized before use by 1 M HCl. The total 4αGT activity of 12 nM *Par*GT was determined on 500 μL amylose (3 mg/mL) in 100 mM citrate-phosphate pH 5.5 (75 °C, 1 min). The reaction was stopped by adding 3 M Na_2CO_3 (0.3 M final concentration), and residual amylose was quantified by mixing 20 μL reaction with 200 μL iodine reagent (0.2% KI + 0.02% I_2), using amylose (0.1–5 mg/mL) as standard. After 1 min, the absorbance was measured at 620 nm (microplate reader, PowerWave XS, BIO-TEK). One unit (U) of total activity was defined as the amount of enzyme degrading 0.5 mg/mL amylose per min under these conditions.

2.5. Kinetics on soluble substrate

Kinetic constants for disproportionation of G3 and degradation of amylose were determined under standard conditions (see 2.4.2. and 2.4.4.). Glucose release and loss of amylose were determined in the substrate concentration ranges 1–200 mM G3 and 0.1–5 mg/mL amylose, respectively. The K_M, k_{cat} and k_{cat}/K_M were calculated by fitting the data with the Michaelis-Menten (MM) equation using the nonlinear regression using Graph Pad Prism v10 (GraphPad Software Inc., San Diego, CA, USA).

2.6. Disproportionation products analysis

*Par*GT (12 nM) was incubated with 40 mM G3-G7 in 100 mM citrate-phosphate pH 5.5 (75 °C, 30 min, agitated at 500 rpm). The reaction was stopped on dry ice and centrifuged (13,000 *g*, 3 min). The products were analysed by high-performance anion exchange chromatography with pulsed amperometric detection (HPAEC-PAD) by Dionex ICS-6000 (Thermo Fisher Scientific, USA) equipped with a Dionex CarboPac PA200 column, injecting 25 μL sample, using a flow rate of 0.5 mL/min and isocratic elution of 80 mM NaOH for 6 min, followed by linear gradient elution of 0–160 mM sodium acetate in 80 mM NaOH for 24 min.

2.7. Differential scanning fluorimetry (DSF)

Melting temperature of *Par*GT (2 μM) was determined using NanoDSF (Prometheus Panta instrument, NanoTemper Technologies,

München, Germany) in 100 mM sodium citrate pH 3.5, pH 4.5, and pH 5.5; phosphate-buffered saline (PBS) composed of 20 mM phosphate and 150 mM NaCl pH 7.3; 100 mM citrate-phosphate at pH 5.5; 20 mM HEPES 200 mM NaCl pH 7.3, and 20 mM HEPES 100 mM NaCl at pH 6.5, pH 7.3, and pH 8.5. *Par*GT, loaded into high sensitivity glass capillaries (Cat#PR-C006, NanoTemper Technologies, München, Germany), was subjected to a temperature ramp from 25 to 100 °C, heating at 1 °C/min. Fluorescence was monitored at 330 and 350 nm upon excitation at 280 nm.

2.8. Preparation of modified HAS granules

HAS granules (Table 1) (6%) were treated with *Par*GT (32 U (2.4.1.)/g starch) in 33 mL 100 mM citrate-phosphate pH 5.5 (75 °C, 24 h, agitated at 1000 rpm) (Wang, Pang, et al., 2024). Three samples are referred to for each of the four HAS: native (N) in the citrate-phosphate pH 5.5 (22 °C, 24 h, agitated at 1000 rpm), as control of buffer incubation effects; blank (B) incubated under reaction conditions (75 °C, 24 h, 1000 rpm) without *Par*GT as control for thermal treatment; reaction (R) presenting incubation combined effects of buffer, heat- and *Par*GT-modification. The 12 samples accordingly are: AE-N, AE-B, AE-R; AOB-N, AOB-B, AOB-R; HAWS-N, HAWS-B, HAWS-R; and HPPS-N, HPPS-B, HPPS-R (Table 2).

2.9. Surface chain length distribution (CLD)

HAS granules (50 mg/mL) suspended in 50 mM sodium acetate pH 4.5, were debranched by pullulanase (50 nM, 25 °C, 1 h, agitated at 1000 rpm), and centrifuged (10,000 *g*, 10 min). Supernatants (100 μL) were analysed by HPAEC-PAD using Dionex (ICS-5000+, ThermoFisher Scientific, USA) equipped with a Dionex CarboPac PA-200 column (Wang, Tian, et al., 2024). Relative content of individual chain lengths was calculated from the specific peak areas. The data provided comparison of the DP distribution of branches in the starches (Tian, Liu, et al., 2024). Average DP was calculated from the values of the relative glucose units of each chain (Zhong et al., 2020).

2.10. Molecular weight distribution

The size distribution of both whole and debranched starch granules chains were analysed as described previously (Wang et al., 2020) with minor modifications. Starch (20 mg) suspended in 1 mL DMSO/LiBr (0.5% *w*/w, Avantor, US) was gelatinized (80 °C, 18 h, agitated at 300 rpm), precipitated by adding 10 mL 96% ethanol and centrifuged (3500 *g*, 10 min). The pellet was resuspended in 1 mL 50 mM sodium acetate, 5 mM $CaCl_2$ pH 4.0 and centrifuged (20,000 *g*, 30 min). The molecular weight distribution of starch α-glucans was determined by size exclusion chromatography with refractive index detector (SEC-RI, UltiMate 3000 UHPLC, ThermoFisher Scientific, USA) injecting 100 μL supernatant on the Ohpak SB-806 M HQ column and using 0.1 M sodium acetate (0.02% NaN_3) as the mobile phase, at a flow rate of 0.5 mL/min and column temperature of 50 °C. The size distribution of α-glucan molecules after debranching was evaluated by incubating the supernatant (1 mL) of the above resuspended pellets with 0.8 U pullulanase (40 °C, 3 h, agitation at 300 rpm). The reaction was stopped by boiling (99 °C, 10 min), centrifuged (20,000 *g*, 30 min) and the supernatant (100 μL) was analysed by SEC-RI as above. A calibration curve was built using dextran standards in the range of 300 Da to 80 kDa. Data were analysed by ASTRA software version 5.3.4 (Wyatt Technologies).

Table 2
Experimental design for *Par*GT modification of AE, AOB, HAWS and HPPS high amylose starches in 100 mM citrate-phosphate buffer pH 5.5 for 24 h.

Sample[1]	Temperature (°C)	*Par*GT (U/g starch)
Native		
AE-N	22	–
AOB-N	22	–
HAWS-N	22	–
HPPS-N	22	–
Blank		
AE-B	75	–
AOB-B	75	–
HAWS-B	75	–
HPPS-B	75	–
Reaction		
AE-R	75	32
AOB-R	75	32
HAWS-R	75	32
HPPS-R	75	32

[1] For sample abbreviations see Table 1 and Section 2.8.

2.11. Wide-angle X-ray scattering (WAXS)

Starch granules were exposed to 90% relative humidity (RH) for 48 h before analysing crystalline allomorphs and relative crystallinity using a Nano-inXider instrument with Cu-Kα radiation using a wavelength of 0.1542 nm (Xenocs SAS, Grenoble, France). Radially averaged intensity (I) was plotted against scattering angle (2θ) between 5° and 40°. Relative crystallinity was calculated using established methods (Brückner, 2000) by using the PeakFit software (version 4.12).

2.12. Fourier transform infrared-attenuated total reflectance (FTIR-ATR) spectroscopy

Surface molecular order was assessed by FTIR-ATR that informs on the organisation in the starch granule to a depth of about 2 μm (Sevenou et al., 2002; Warren et al., 2016). Measurements were performed on starch samples equilibrated to 90% RH prior to analysis to ensure consistent surface hydration prior analysis. Spectral data were acquired using a Shimadzu IRSpirit-X FTIR spectrometer (Shimadzu, Kyoto, Japan) equipped with the QATR-S attenuated total reflectance (ATR) accessory. Spectra for each sample were combined, by co-adding at a resolution of 4 cm^{-1}, with a background spectrum collected through 128 co-added scans (Tian, Liu, et al., 2024). A Lorentzian line shape, with a half-width of 19 cm^{-1} and a resolution enhancement factor of 1.9, was assumed. Following baseline correction and deconvolution, IR absorbance values at 1022 and 1045 cm^{-1}, indicative of double-helical organisation (Warren et al., 2016), were extracted from the spectra using OMNIC software (Capron et al., 2007).

2.13. Scanning electron microscopy (SEM)

The starch granules were washed with MilliQ water and freeze-dried. For imaging, the starch granules were mounted on carbon tapes on aluminium SEM stubs and sputter-coated with 6 nm gold under a Leica EM ACE200 gold coater (Leica Microsystems, Wetzlar, Germany). Both overall and detailed morphology of HAS—N, HAS-B and HAS-R granular starch samples were visualized using field emission scanning electron microscopy (FE-SEM; FEI Quanta 200 microscope) at 1000×, 5000× and 10,000× magnification, respectively, essentially as previously described (Tian et al., 2023; Wang, Tian, et al., 2024).

2.14. In vitro digestibility

Starch granules (20 mg), suspended in 2 mL 50 mM sodium acetate, 5 mM $CaCl_2$, pH 5.5, were degraded by 2 mg/mL pancreatin, containing porcine pancreatic α-amylase (PPA), and 3.6 μM *Aspergillus niger* glucoamylase (GA) (both final concentrations) (37 °C, 2 h, agitated at 300 rpm) (Wang, Pang, et al., 2024). Aliquots of 50 μL were removed at 0, 5, 10, 15, 20, 30, 60, 90, 120 and 180 min, mixed with 95% ethanol (500 μL) and centrifuged (10,000 *g*, 5 min). Glucose in the supernatants was

quantified using the GOPOD assay (see 2.4.1.) with glucose as standard (0.5–5.5 mM) (Huggett & Nixon, 1957). Rapidly digested starch (RDS) was defined as the starch fraction converted to glucose at 0–20 min, slowly digested starch (SDS) at 20–120 min, and resistant starch (RS) as the remaining residue (Englyst et al., 1992):

$$\%RDS = G20/(\text{initial dry mass of sample}) \times (162/180) \times 100\%$$

$$\%SDS = (G120 - G20)/(\text{initial dry mass of sample}) \times (162/180) \times 100\%$$

$$\%RS = 100\% - (\%RDS + \%SDS)$$

2.15. Langmuir adsorption onto starch granules

HAS (15 mg/mL) was incubated with 0.1–10 μM GA (37 °C, 10 min, agitated at 1100 rpm) and centrifuged (10,000 *g*, 5 min). The supernatant (100 μL) was mixed with 100 μL 2.5-fold diluted Protein Assay Dye Reagent (Bio-Rad) and the GA concentration (E_{free}, in nM) was determined from the absorbance ratio at 590 nm and 450 nm using bovine serum albumin (BSA, Sigma) as standard. Data were fitted to the *Langmuir* isotherm (Eq. 1), where K_d (in nM) represents the dissociation constant and ${}^{ads}\Gamma_{max}$ (nmol/g) the density of binding sites, also referred to as the (apparent) saturation coverage (Kari et al., 2018).

$$\Gamma = \frac{{}^{ads}\Gamma_{max} \cdot E_{free}}{K_d + E_{free}} \quad (1)$$

2.16. Interfacial kinetics analysis of GA hydrolysis of granular starch

Two complementary methods, conventional and inverse Michaelis-Menten (MM) analyses, were employed to characterize the kinetics of granular starch hydrolysis by GA. For conventional MM analysis, 135 μL of seven different concentrations of starch granules (15–150 mg/mL) were pre-incubated (37 °C, 10 min, agitated at 1100 rpm) and the reaction was initiated by addition of 0.7 nM GA (final concentration). For inverse MM kinetics analysis, starch granules (135 μL, 15 mg/mL) were mixed with 15 μL of seven final GA concentrations (10–5000 nM). After incubation within the linear reaction range (37 °C, 30 min, agitated at 1100 rpm; data not shown) for both MM procedures, 30 μL 1.8 M Na_2CO_3 was added to terminate the reaction followed by centrifugation (10,000 *g*, 5 min). Reducing sugar in the supernatant was quantified using the PAHBAH method with glucose (0–1 μM) as standard (Lever et al., 1973).

Conventional MM data were analysed using equation (Eq. 2) for nonlinear regression analysis where S_0^{mass} is substrate mass load and $K_{1/2}$ the mass load at substrate half-saturation (in $g{\cdot}L^{-1}$) and V_{max} (in $M{\cdot}s^{-1}$) (Kari et al., 2018).

$$v_0 = \frac{V_{max} \cdot S_0^{mass}}{K_{1/2} + S_0^{mass}} \quad (2)$$

Inverse MM data were analysed using equation (Eq. 3) by nonlinear regression analysis to give the parameters ${}^{inv}V_{max}$ (in $g{\cdot}L^{-1}{\cdot}s^{-1}$), E_0 is the enzyme concentration and ${}^{inv}K_M$ the concentration of enzyme at half saturation (in M).

$$v_0 = \frac{{}^{inv}V_{max} \cdot E_0}{{}^{inv}K_M + E_0} \quad (3)$$

The attack site density (${}^{kin}\Gamma_{max}$ in nmol/g) was calculated by Eq. 4 using V_{max} (Eq. 2) and ${}^{inv}V_{max}$ (Eq. 3) (Kari et al., 2018).

$$\frac{\frac{{}^{inv}V_{max}}{S_0^{mass}}}{\frac{V_{max}}{E_0}} = {}^{kin}\Gamma_{max} \quad (4)$$

2.17. Statistical analysis

All experiments were performed in duplicate. The statistical significance was assessed with one-way analysis of variance (ANOVA) using SPSS 20.0 (SPSS Inc., Chicago, USA). Differences were considered statistically significant at $p < 0.05$. Correlations were analysed using Pearson's correlation through the "cor" function and visualized with the R package "corrplot" (Wei & Simko, 2017).

3. Results and discussion

3.1. Bioinformatic analysis

The metagenomic dataset from the Pisciarelli solfatara in Naples (Italy) (Strazzulli et al., 2020) led to the identification of a gene encoding an archaeal glycoside hydrolase, initially named GH77_pool1, belonging to family GH77 in the CAZy database classification (https://www.cazy.org; Drula et al., 2022). Blast analysis revealed 100% identity score of GH77_pool1 with *Par*GT, a 4αGT from *Pyrobaculum arsenaticum* (Jung et al., 2025). Moreover, it showed 75.96% maximum similarity with 4αGT from *Pyrobaculum aerophilum* str. IM2 (Kaper et al., 2005) and 65.54% with 4αGT from *Thermoproteus uzoniensis* 768–20 (Wang et al., 2020). *Par*GT possessed the typical GH77 conserved sequence regions, including three putative catalytic residues; the nucleophile Asp271 in conserved region I, the proton donor Glu318 in conserved region II, and the transition-state stabilizer Asp371 in conserved region III (Fig. S1). The structural model generated by AlphaFold3 and analysed using PyMol, showed the $(\beta/\alpha)_8$-barrel fold typical of family GH77 and clan GH-H (Przylas et al., 2000) (Fig. S2). Interestingly, the predicted structure of *Par*GT lacks an α-helical element observed in the available 4αGT crystal structures, likely due to a gap of 13 amino acid residues in the *Par*GT sequence starting at position 158 (Fig. S3).

3.2. Production and purification of ParGT

Recombinant *Par*GT was produced in *E. coli* and purified in yields of 1 mg per litre of culture. The molecular mass of *Par*GT was 56 kDa as determined by SDS-PAGE, in agreement with the theoretical molecular mass of 54,381 Da. Analytical SEC indicated *Par*GT to be a tetramer of 225 ± 25 kDa in 25 mM HEPES, 100 mM NaCl, pH 7.3.

3.3. Activity and kinetics on MOS and amylose

*Par*GT catalysed disproportionation of G3 with a specific activity of 1170 ± 12 U/mg at 75 °C in 100 mM citrate-phosphate pH 5.5. Highest activity was obtained at 100 °C (Fig. 1A) and pH 5.5 (Fig. 1B) and 65% activity was retained after 4 h at 75 °C (Fig. 1C). Jung et al. (2025) reported very similar optimal conditions of 95 °C and pH 6.0 for *Par*GT using slightly different storage and assay conditions. Notably, *Par*GT stored in 25 mM HEPES, 100 mM NaCl, pH 7.3 showed 5-fold higher activity on G3 (1170 U/mg) than by storage in PBS (20 mM NaH_2PO_4, 150 mM NaCl pH 7.3) (230 U/mg), which also resulted in a slightly lower optimal temperature of 95 °C (Fig. S4). This prompted examination of *Par*GT stability in different buffer systems by nanoDSF melting temperature analysis (Fig. S5). *Par*GT showed maximum stability of the folded state in HEPES at 100 and 200 mM NaCl, pH 6.5–7.3, but not in PBS pH 7.3. The findings showed a strong link between storage buffer composition, activity and thermophilicity of *Par*GT underlining the critical role of pH, buffer components, and assay conditions in preserving enzyme stability and activity. *Par*GT is the most thermophilic 4αGT reported to date, exhibiting highest activity at 100 °C, compared to 90 °C of the previously characterised 4αGT from *Aquifex aeolicus* (Bhuiyan et al., 2003) and 95 °C of 4αGT from *Pyrobaculum aerophilum* (Kaper et al., 2005). Notably, members of the genus *Pyrobaculum* are known to grow optimally at 100 °C, thus the temperature optimum of

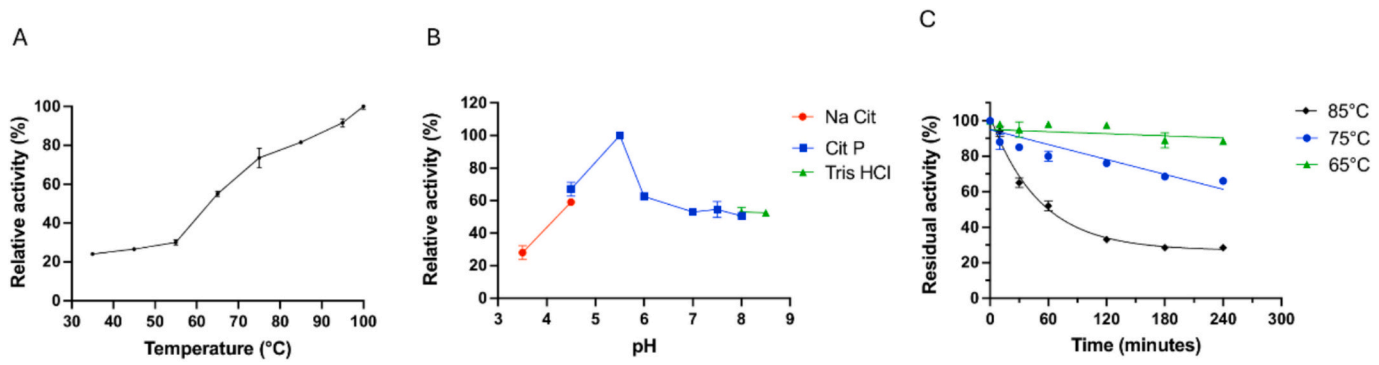

Fig. 1. Optimal conditions for activity and stability of *Par*GT. (A) Temperature optimum. (B) pH dependence. (C) Thermal stability at 65, 75, 85 °C.

*Par*GT is finely tuned for extreme thermal conditions, likely reflecting the environmental pressure of its archaeal habitat origin (Huber et al., 2000; Strazzulli et al., 2020).

Understanding the response of enzymes to metal ions is particularly relevant for biotechnological applications for example in starch-based biofilms, where antimicrobial metal additives (Zn^{2+}, Cu^{2+}) are commonly used (Ślosarczyk et al., 2023). The disproportionation activity of *Par*GT was not affected by 5 mM K^{+}, Na^{+}, Cu^{2+}, Ca^{2+}, Fe^{3+}, Mg^{2+}, Mn^{2+} and Zn^{2+} (Fig. S6A), but 20 mM Fe^{3+} inhibited *Par*GT and 40 mM Zn^{2+} significantly reduced the activity (Fig. S6B,C). Notably, 40 mM Mn^{2+} enhanced activity by about 20% (Fig. S6C). These effects reflected a trend observed for certain glycoside hydrolases and transferases of Fe^{3+} and Zn^{2+} causing significant inhibition by interacting with thiol or carboxylate groups and disrupting the active site (Ashraf et al., 2022; Chen et al., 2018; Demirkan et al., 2005; Kaper et al., 2005; Mehboob et al., 2020), suggesting a role of cysteines in *Par*GT stability. Conversely, Mn^{2+} often acts as a structural cofactor enhancing activity (Alarico et al., 2008; Seo et al., 2011).

The steady-state kinetic parameters for disproportionation of G3 and degradation of amylose by *Par*GT were determined under standard assay conditions. *Par*GT has higher activity on G3 (k_{cat} 2042 ± 23 s^{-1}, K_M 17.0 ± 0.1 mM, k_{cat}/K_M 118 mM^{-1} s^{-1}) than the characterised archaeal GH77 4αGTs MalQ (k_{cat}/K_M 31 mM^{-1} s^{-1}) (Kaper et al., 2005); and *Tu*αGT (k_{cat}/K_M 0.03 mM^{-1} s^{-1}) (Wang et al., 2020). Moreover, *Par*GT showed high affinity for amylose (k_{cat} 18.0 ± 2 4 s^{-1}, K_M 0.4 ± 0.1 mg/mL, k_{cat}/K_M 44.0 mg/mL^{-1} s^{-1}). 4αGTs in transfer reactions generate α-glucan segments starting from G3, by balancing essential *in vivo* degradation and synthesis of α-glucans in the carbohydrate metabolism (Cifuente et al., 2024; Kamerling, 2007; Wang et al., 2019). Beyond the physiological role, disproportionation by 4αGTs presents opportunities for biotechnological applications, such as starch modification, and in synthesis of functional oligosaccharides (Chen et al., 2023; Leoni et al., 2021).

The disproportionation by *Par*GT of G3-G7 resulted in products of higher DP than the substrates (Fig. 2A, peaks in black boxes). The highest activity was on G3, followed by G4, G5, G6, and G7 in that order, confirming the substrate preference pattern reported by Jung et al. (2025) (Fig. 2B). No maltose was detected, indicating that *Par*GT exclusively catalysed transglycosylation. Thus, maltose from G3 donor, transglycosylates G3, with G3-G7 substrates and their reaction products as both initial donor and acceptor, eventually yielding larger MOS (Fig. 2A, Table 3). Notably, *Par*GT produced longer MOS from G3-G7 than thermophilic 4αGTs from *P. aerophilum* and *T. uzoniensis*. Specifically, *Par*GT generated products up to around DP16, while the 4αGTs of *T. uzoniensis* (Wang et al., 2020) and *P. aerophilum* (Kaper et al., 2005) formed MOS with higher DP of 7 and > DP 9, respectively. This indicated superior ability of *Par*GT for α-glucan chain elongation from MOS by transfer either of larger α-glucan segments or repeated transfer of

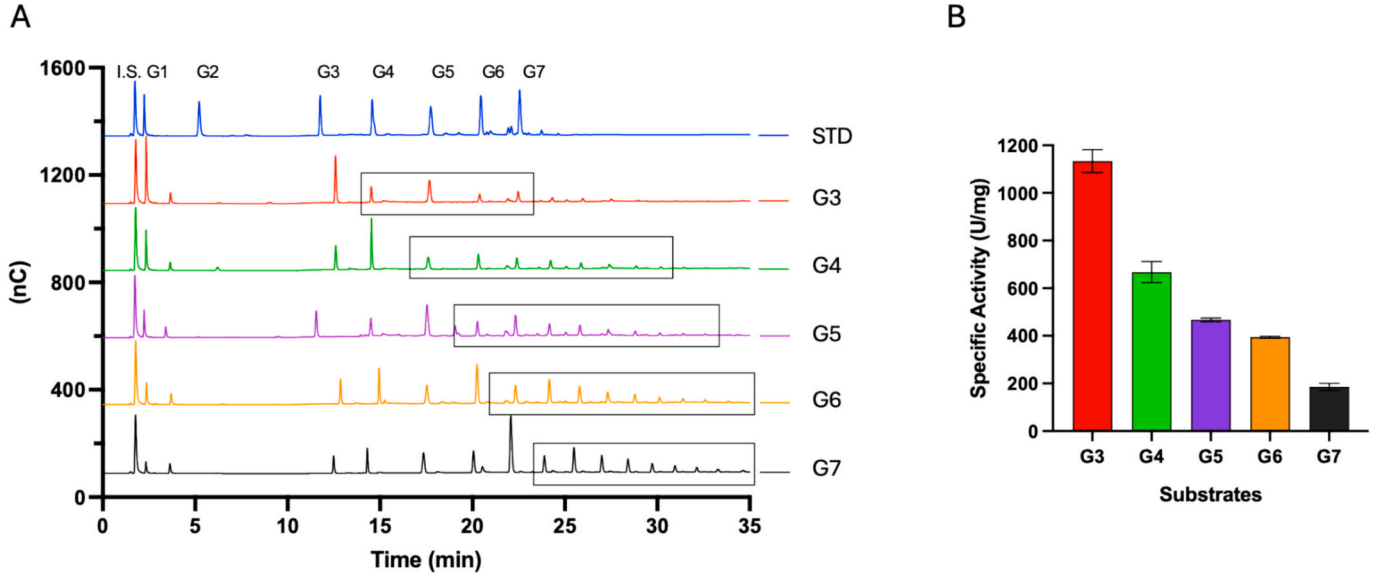

Fig. 2. *Par*GT disproportionation reactions on G3-G7. (A) HPAEC-PAD elution profiles showing *Par*GT elongated products (in black boxes). Standards (blue): I.S. (trehalose as internal standard). G1, glucose. G2, maltose. G3, maltotriose. G4, maltotetraose. G5, maltopentaose. G6, maltohexaose. G7, maltoheptaose. (B) Specific activity of *Par*GT on G3–G7.

Table 3
Disproportionation products of *Par*GT and two other archaeal 4αGTs acting on maltooligosaccharides (DP3–7)[1].

Substrate	Main products (DP)		
	Pyrobaculum arsenaticum (This study)	*Pyrobaculum aerophilum* (Kaper et al., 2005)	*Thermoproteus uzoniensis* (Wang et al., 2020)
G3	1; 3–7	1; 5	1–5
G4	1; 3–12	1; 7	1–6
G5	1; 3–14	3; 7	n.d.
G6	1; 3–15	3; >9	n.d.
G7	1; 3–16	3; 4; >9	n.d.

n.d.: not detected.
[1] G3, maltotriose; G4, maltotetraose; G5, maltopentaose; G6, maltohexaose; G7, maltoheptaose.

shorter units or both. The strong affinity and rapid turnover, thus high catalytic efficiency (k_{cat}/K_M), of *Par*GT in G3 disproportionation aligned with its ability to produce longer products (Table 3), which is favourable for extensive α-glucan remodelling.

3.4. Experimental setup for the granular HAS modification

The *Par*GT activity was assessed within the time range of the modification, and up to about 50% activity was retained under the applied conditions (Fig. S7). Sets of three HAS samples were prepared in these experiments: native, granules incubated in reaction buffer at 22 °C without *Par*GT (HAS-N); blank, granules incubated at 75 °C in the buffer also without *Par*GT (HAS-B); and reaction, granules treated at 75 °C in the buffer with *Par*GT (HAS-R). HAS-N and HAS-B served as buffer- and thermal-treatment control, respectively. Supernatants and pellets were analysed separately for the 12 incubated samples, corresponding to the three conditions, native, blank, and reaction, for each of the four types of HAS granules (Table 2).

3.4.1. Soluble products produced from HAS granules by ParGT

HAS-R, HAS-B and HAS-N supernatants were examined (Supplementary experimental Sections 1.1 and 1.2) by MALDI-TOF/TOF for formation of cyclic MOS and by HPAEC-PAD to describe DP of linear MOS released from the granules (Fig. S8). After GA treatment no cyclodextrins or large-ring cyclodextrins were detected by MALDI-TOF/TOF (data not shown) and only linear MOS were found in the supernatants. Notably, DP of the *Par*GT soluble products released from the granules was up to 45 for AE-R and AOB-R (Fig. S8A, B), DP25 for HAWS-R, and DP60 for HPPS-R (Fig. S8C, D). This indicated that *Par*GT catalysed disproportionation on the granular surface releasing soluble products of different lengths. Moreover, depending on the starch type, different soluble products were also released from HAS-N and HAS-B samples. This suggests that *Par*GT catalysed disproportionation both on the granule surface and on the solubilized oligosaccharides generated during the resuspension of the granules whether at room temperature (HAS—N) or after heating (HAS—B), as reflected by the differences observed between the HAS-B and HAS-R profiles (Fig. S8).

3.4.2. Surface chain length distribution

The *Par*GT modification of HAS granules was assessed by chain length distribution (CLD) analysis following pullulanase-mediated debranching of the surfaces (Wang, Tian, et al., 2024). The CLD changed significantly in HAS-B and HAS-R compared to HAS-N samples, as evidenced by the relative amounts of A (DP 1–12), B1 (DP 13–24), B2 (DP 25–36) and B3 (DP ≥ 37) chains (Bertoft, 2017; Bertoft et al., 2024) (Table 4). The CLD data of *Par*GT modified starch granules (HAS-R) revealed structural rearrangements across AE and HPPS indicated by the relative amounts of A, B1, B2 and B3 chains compared to the HAS-N granules (Fig. 3A,C, Table 4). Specifically, in native AE granules (AE-N), A-chains (DP 1–12) accounted for nearly 70% of all chains, while

Table 4
Percentage of surface branch chain length categories of HAS granules.

Granular HAS[1]	Type of chain				Average DP
	A-chain (DP 1–12)	B1-chain (DP 13–24)	B2-chain (DP 25–36)	B3-chain (DP > 37)	
AE - N	69.7 ± 1.5 [a2]	19.7 ± 0.8 [c]	7.9 ± 0.7 [b]	2.7 ± 0.1 [b]	9.7 ± 0.6 [b]
AE - B	28.5 ± 0.5 [c]	52.6 ± 0.6 [a]	11.8 ± 0.3 [a]	3.0 ± 1.0 [b]	16.9 ± 1.5 [a]
AE - R	37.0 ± 0.5 [b]	47.9 ± 0.1 [b]	9.0 ± 0.3 [b]	6.1 ± 0.2 [a]	17.0 ± 0.1 [a]
AOB - N	57.3 ± 1.5 [a]	31.3 ± 2.1 [b]	11.0 ± 0.1 [a]	n.d. [3]	12.8 ± 0.3 [b]
AOB - B	31.1 ± 0.5 [b]	50.8 ± 0.2 [a]	10.5 ± 0.1 [b]	7.6 ± 0.5 [a]	18.4 ± 0.2 [a]
AOB - R	31.4 ± 0.2 [b]	51.0 ± 0.3 [a]	10.5 ± 0.2 [b]	7.1 ± 0.3 [a]	18.3 ± 0.0 [a]
HAWS - N	99.7 ± 0.2 [a]	0.3 ± 0.2 [c]	n.d.	n.d.	2.3 ± 0.03 [b]
HAWS - B	17.4 ± 0.05 [b]	46.5 ± 0.1 [a]	18.8 ± 0.5 [a]	17.3 ± 0.3 [b]	24.3 ± 0.0 [ab]
HAWS - R	17.3 ± 0.05 [b]	45.4 ± 0.5 [b]	18.7 ± 0.1 [a]	18.5 ± 0.4 [a]	24.8 ± 0.2 [a]
HPPS- N	54.3 ± 1.9 [a]	42.2 ± 0.5 [c]	3.5 ± 1.4 [b]	n.d.	11.4 ± 0.7 [b]
HPPS - B	10.7 ± 3.4 [c]	66.3 ± 2.7 [a]	16.3 ± 1.0 [a]	8.7 ± 1.0 [b]	23.0 ± 1.5 [a]
HPPS - R	17.2 ± 0.2 [b]	50.3 ± 0.1 [b]	14.6 ± 0.01 [a]	17.9 ± 0.2 [a]	24.3 ± 0.0 [a]

n.d.: not detected.
[1] For sample abbreviations see Table 1 and Section 2.8.
[2] Values with different letters within the three types of the same HAS in the same column are significantly different at $p < 0.05$.

smaller proportions were found of B1-, B2-, and B3-chains. For AE-B, the A-chains decreased drastically from 69.7% to 28.5% while B1-chains increased from 19.7% to 52.6%, indicating heat-induced rearrangement, likely uncoiling and exposing longer branches on the surface to be cleaved off by pullulanase (Fonseca et al., 2021). However, *Par*GT-modification (AE-R) slightly increased the content of A-chains compared to AE-B, and B3-chains about 2-fold compared to AE-N and AE-B. This may be described by a simplification assuming that *Par*GT used B1-chains as donors and other branches (A, B2, B3) as acceptors. AOB showed a comparable trend for AOB-N displaying mostly A- and no B3-chains, but B3-chains (7.6%) became exposed by heating in AOB-B and released by pullulanase. Notably, AOB-R and AOB-B gave nearly identical CLD, indicating limited *Par*GT modification, suggesting restricted *Par*GT access post-heating. CLD of HPPS-B differed greatly from HPPS-N, by A-chains being reducing from 54.3% (HPPS-N) to 10.7% (HPPS-B) along with large increases of B1, B2, and B3, indicative of heat-induced access to debranching by pullulanase. B3-chains were further increased (~18%) in HPPS-R (Table 4), clearly reflecting *Par*GT-catalysed elongation and rearrangement reactions, beyond the thermal effects, as also found for AE. Thus, in both AE and HPPS *Par*GT restructured α-glucan chains by disproportionation extending exterior branch chains of amylopectin. This behaviour is consistent with previous reports that 4αGTs alter branch chain length distributions of different gelatinised/slurry starch sources (Cho et al., 2009; Jiang et al., 2014; van der Maarel et al., 2005). Notably, however, a different CLD pattern was observed for AE when treated with a 4αGT from *T. uzoniensis* (Wang et al., 2020), which produced a higher proportion of DP 1–3 at the expense of the DP 4–12 fraction (Wang, Tian, Rennison, et al., 2025). This contrast highlights enzyme-specific behaviour on the same granular substrate: *Par*GT (this study) promoted branch elongation under high-temperature (75 °C), sub-gelatinisation conditions, whereas the *T. uzoniensis*

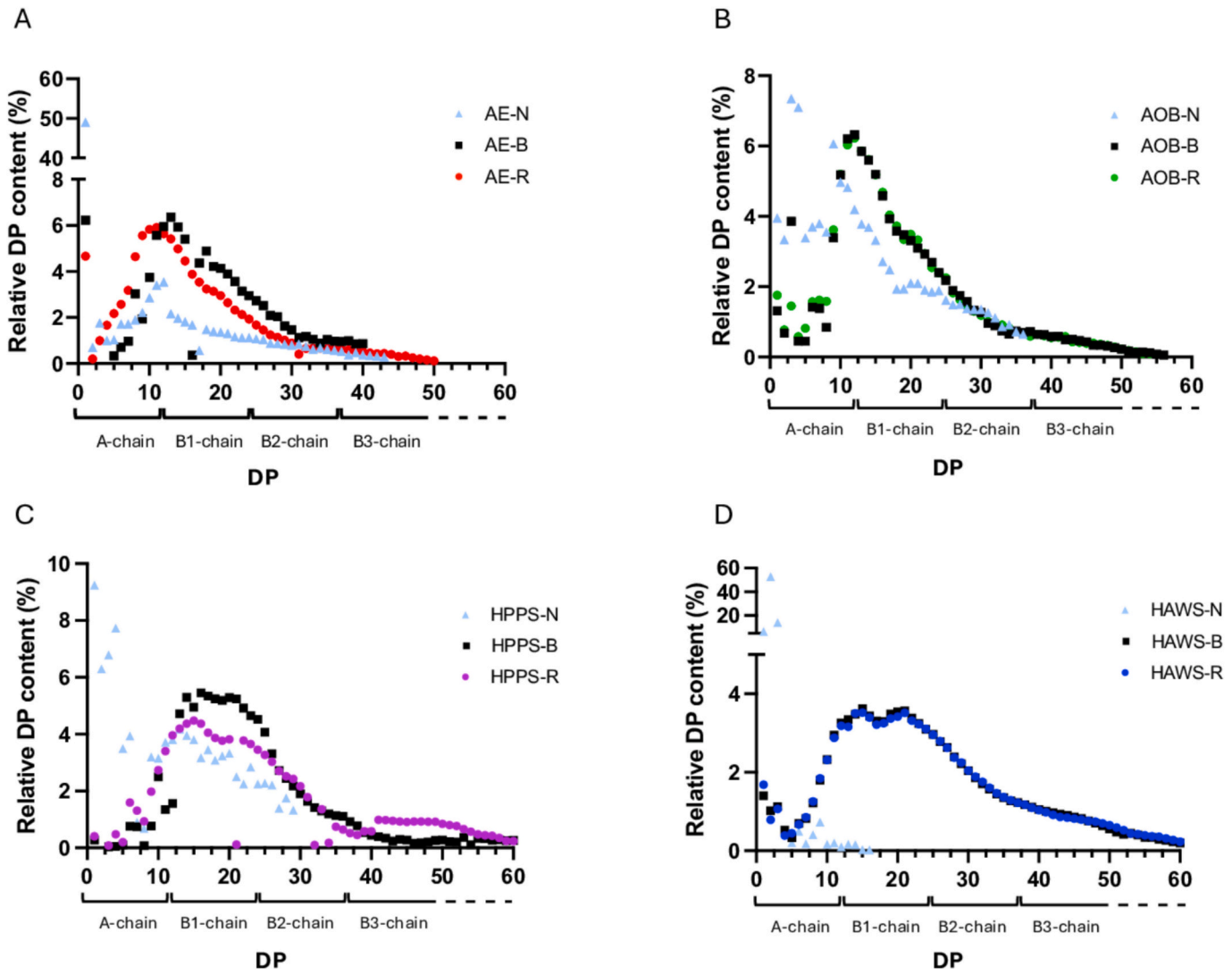

Fig. 3. Surface chain length distribution of *Par*GT-modified HAS granules. (A) AE, (B) AOB, (C) HPPS, (D) HAWS. The DP for CLD of enzymatically modified starches (R) is shown in red (AE), green (AOB), purple (HPPS), and bright blue (HAWS). Light blue triangles and black squares indicate CLD of native HASs (N) and heat-treated blank HASs (B), respectively. For sample abbreviations see Table 1 and Section 2.8.

enzyme produced a relative increase in very short chains by treatment at the milder temperature of 50 °C.

HAWS (Fig. 3D) behaved similarly to AOB (Fig. 3B) by almost only A-chains being released by debranching of HAWS-N, while significant

Table 5
Degree of surface order (1047 cm^{-1}/1022 cm^{-1}), content of amorphous and crystalline regions, and crystallinity type of different HAS granules.

Sample[1]	FTIR ratio (1047 cm^{-1}/1022 cm^{-1})	Amorphous (%)	Crystalline (%)	Crystallinity		
				V-type (%)	B-type (%)	A-type (%)
AE-N	0.61 ± 0.0 [c2]	79.7 ± 1.0 [b]	21.0 ± 1.0 [b]	7.4 ± 0.2 [b]	10.8 ± 0.2 [a]	n.d. [3]
AE-B	0.64 ± 0.0 [b]	79.6 ± 1.1 [b]	21.4 ± 0.4 [a]	8.1 ± 0.2 [a]	6.8 ± 0.5 [b]	n.d.
AE-R	0.68 ± 0.0 [a]	81.8 ± 0.4 [a]	18.2 ± 0.4 [c]	6.8 ± 0.4 [c]	5.7 ± 0.2 [c]	n.d.
AOB-N	0.46 ± 0.0 [a]	76.3 ± 0.1 [c]	23.7 ± 0.1 [a]	18.5 ± 2.1 [a]	3.4 ± 0.0 [a]	n.d.
AOB-B	0.43 ± 0.0 [b]	83.2 ± 0.1 [a]	16.8 ± 0.1 [c]	15.0 ± 0.4 [c]	1.0 ± 0.2 [c]	n.d.
AOB-R	0.44 ± 0.0 [b]	79.2 ± 0.1 [b]	20.8 ± 0.1 [b]	16.9 ± 0.5 [b]	2.1 ± 0.4 [b]	n.d.
HPPS-N	0.64 ± 0.01 [b]	76.0 ± 1.2 [c]	24.0 ± 1.2 [a]	4.8 ± 1.6 [a]	14.0 ± 0.6 [a]	n.d.
HPPS-B	0.63 ± 0.0 [b]	77.7 ± 0.0 [b]	22.2 ± 0.2 [b]	3.0 ± 0.0 [b]	14.6 ± 0.1 [a]	n.d.
HPPS-R	0.69 ± 0.0 [a]	84.1 ± 0.7 [a]	16.2 ± 0.3 [c]	1.9 ± 0.0 [c]	8.7 ± 0.7 [b]	n.d.
HAWS-N	0.51 ± 0.0 [b]	85.8 ± 0.3 [b]	14.2 ± 0.3 [a]	5.1 ± 0.9 [a]	3.7 ± 0.1 [a]	2.4 ± 0.4 [a]
HAWS-B	0.52 ± 0.01 [b]	89.3 ± 0.8 [a]	10.7 ± 0.8 [b]	4.3 ± 0.3 [a]	3.1 ± 0.0 [b]	1.7 ± 0.2 [a]
HAWS-R	0.64 ± 0.04 [a]	88.8 ± 1.0 [a]	11.2 ± 1.0 [b]	4.9 ± 0.1 [a]	3.2 ± 0.4 [b]	2.0 ± 0.6 [a]

n.d.: not detected.
[1] For sample abbreviations see Table 1 and Section 2.8.
[2] Values with different letters within the three types of the same HAS in the same column are significantly different at $p < 0.05$.

amounts of B1, B2 and B3 emerged in HAWS-B and HAWS-R with essentially superimposable CLD patterns (Fig. 3D, Table 4). Thus, at first glance, it seemed that *Par*GT did not modify the branching structure of HAWS beyond heat treatment, possibly because of a dense architecture, that may also restrict productive access of pullulanase to α-1,6 branch points. However, *Par*GT seemed to influence the surface and/or more of the amorphous regions of HAWS, as supported by FTIR analysis indicating increased short-range molecular order in HAWS-R (Table 5), which is associated with RS formation (Fig. 6). Accordingly, the lack of differences in the CLD patterns of HPPS-B and HPPS-R may be explained by the reassociation of chains into a more compact structure after *Par*GT modification (as indicated by the higher FTIR 1045 cm^{-1}/1022 cm^{-1} ratio in HPPS-R), which restricted pullulanase debranching activity on the surface.

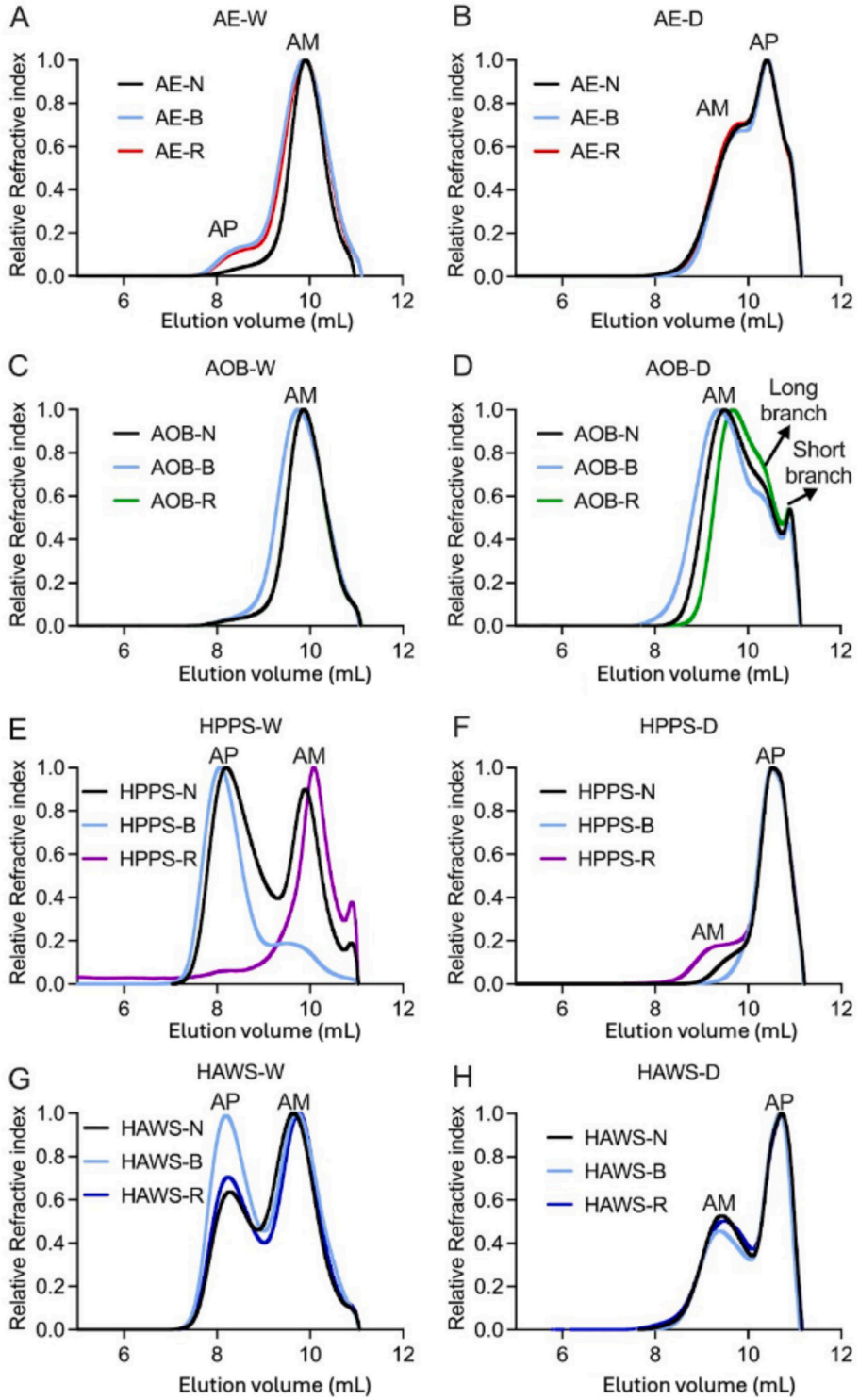

Fig. 4. SEC analysis of molecular size distribution of whole (A, C, E, F) and debranched HAS molecules, showing the α-glucan backbone of AM, AP and longer branches (B, D, F, H). Red (AE), green (AOB) (in panel C, AOB-R overlaps with AOB-N in black), purple (HPPS), and bright blue (HAWS). For sample abbreviations see Table 1 and Section 2.8.

3.4.3. HAS α-glucan molecular size distribution

The molecular size was determined by SEC-RI for the whole (W) and debranched (D) starch molecules. The elution profiles typically have two peaks, one of amylopectin (AP) and one of amylose (AM), except for AOB that lacks AP. Firstly, comparing intact starch molecules (W) of HAS-N and HAS-B samples, AE-B contained slightly more AP than AE-N (Fig. 4A) similar to HPPS-B and HAWS-B, both of which showed significantly higher AP contents than HPPS-N and HAWS-N (Fig. 4E,G). This reflects leaching of AM from the granules during heat treatment, a phenomenon commonly associated with gelatinization (Ji et al., 2022). Previously, Tian et al. (2024) showed that HAWS has the lowest gelatinization onset temperature (54 °C), followed by HPPS (65 °C), AE (84 °C), and AOB (88 °C). Therefore, at 75 °C, used for HAS granules modification, HAWS and HPPS may undergo more severe structural disruption provoking leaching of greater amounts of AM. Differently, AOB-R displayed smaller molecular size than AOB-B (Fig. 4C). As AOB is lacking AP, but the AM can carry a few branches (Zhong et al., 2022), debranching slightly decreased the size of AM and the proportion of long branches increased in AOB-R (Fig. 4D). *Par*GT may catalyse disproportionation with the linear AM backbone as donor and branches existing on AM as acceptors (Fig. 4D). In comparison, the whole (W) HPPS-R and HAWS-R, showed significant increase of molecules eluting later than HPPS-B and HAWS-B (Fig. 4E,G), indicating that *Par*GT-treatment decreased the hydrodynamic radius of the molecules in HPPS-R and HAWS-R (Chen, Wang, et al., 2024), and extensively hydrolysed α-1,4 glucan chains within AP, leading to the production of amylose-like molecules. Debranched HPPS-R and HAWS-R displayed a higher proportion of amylose-like chains (Fig. 4F,H), which likely results from *Par*GT-driven elongation of amylopectin branches. By extending the α-1,4 glucan chains, *Par*GT may partially convert amylopectin-derived fragments into longer, more linear structures that contribute to the apparent amylose fraction. These elongation products (Fig. 4F,H) are too large (up to DP 60) to be analysed by HPAEC-PAD.

3.4.4. Degree of surface order

FTIR-ATR spectra of the HASs granules in the 800–1200 cm^{-1} range, corresponding to C—O and C—C stretching vibrations, provide insights into polymer conformation at the surface (~2 μm depth) (Capron et al., 2007). This analysis, particularly the 1045 cm^{-1}/1022 cm^{-1} ratio, illustrates short-range molecular order at the granular surface, related to the presence of double helices. Notably, analysis of the HAS—N, —B and -R showed clear increase in surface order for AE, HAWS and HPPS by the *Par*GT-treatment (Fig. S9). Thus, the 1045 cm^{-1}/1022 cm^{-1} ratio was raised from 0.61 of AE-N to 0.64 of AE-B and to 0.68 in AE-R (Fig. S9, Table 5). For HAWS, the FTIR ratio at 1045 cm^{-1}/1022 cm^{-1} increased to 0.64 in HAWS-R, compared with much lower values in HAWS-N (0.51) and HAWS-B (0.52) (Table 5). Although this may seem contradictory to the similar HAWS-B and -R CLD profiles (Fig. 3D, Table 4), these patterns seemed to be attributed to the limited pullulanase debranching action, rather than a lack of *Par*GT activity on HAWS granules. Indeed, the higher FTIR 1045 cm^{-1}/1022 cm^{-1} values of HPPS-R compared to HPPS-B (Table 5) confirmed that the *Par*GT activity elicited reorganization of the granule surface. Finally, HPPS-R had even the highest 1045 cm^{-1}/1022 cm^{-1} value of 0.69 (Table 5), in agreement with the increased content of B3 chains (Fig. 3C, Table 4), with longer chains apparently facilitating the rearrangement into more ordered structures. This higher surface order conferred by *Par*GT in AE, HAWS and HPPS was assumed to stem from increased formation of double helices (Fig. S9). Possibly, more mobile linear chains are available under annealing-like conditions, which after the *Par*GT modification realign into ordered structures, such as double helices, indicated by increased 1045 cm^{-1}/1022 cm^{-1} values from the FTIR spectra. The more ordered surface is associated with the *Par*GT disproportionation on HPPS and AE, where CLD showed more long chains (B3). We claim that *Par*GT-modified HPPS and HAWS granules possess features of both type 2 resistant starch (RS2, naturally occurring resistant starch) and type 3 resistant starch (RS3, retrograded resistant starch). By contrast, AOB-N, —B and -R displayed very similar 1045 cm^{-1}/1022 cm^{-1} of 0.46, 0.43, and 0.44, implying that neither heat- nor *Par*GT-treatment affected surface molecular order (Table 5), consistent with the minimal difference in B2, but notably not coherent with the large increase of B3 chains in AOB-B and AOB-R (Fig. 3B, Table 4). This lack of increase in the FTIR ratio, is therefore suggested to reflect that formed longer chains did not re-associate into well-ordered, double-helical structures, likely due to limited granule swelling (Debet & Gidley, 2006; Tian et al., 2025).

3.4.5. Crystalline polymorphs of lamellar structure

WAXS spectra described the lamellar crystalline and amorphous structure of the native and modified HASs which all showed a combination of B-type (at $2\theta = 5.6°$, 17°, 22°, and 26°) and V-type (at $2\theta = 7°$, 13°, 15°, and 20°) crystalline polymorphs, with HAWS also containing A-type (at $2\theta = 23°$) (Table 5, Figs. S10 and S11). Crystallinity trends notably differed across HAS—N, —B, and -R samples (Table 5). The HAS-N samples displayed highest crystallinity, indicative of a well-ordered lamellar architecture prior to the heat-treatment, which generally reduced crystallinity, signifying partial disruption of lamellar crystalline regions (Jacobs & Delcour 1998). Thus, AOB-B, HPPS-B and HAWS-B showed lower crystallinity (16.8%, 22.3% and 10.7%) than their native counterparts (23.7%, 24.0% and 14.2%) (Table 5). Interestingly, *Par*GT-treatment further reduced crystallinity in AE-R and HPPS-R (18.2% and 16.2%) (Table 5), supporting the idea that the enzyme modified internal structures in AE and HPPS, possibly by cleaving and rearranging chains within semi-crystalline regions. Notably, AOB behaved differently, and AOB-R gained some of the crystallinity (20.8%) that was lost by heating the starch granules (AOB-B) (16.8%), albeit still below the level in AOB-N (23.7%) (Table 5). This suggested reorganization of starch chains after *Par*GT-modification following initial heat-induced loosening of crystalline structures of the lamella where amorphous structures seemed to be targeted first (Chen, Qiu, et al., 2024). HAWS showed lowest overall crystallinity across treatments, and minimal variation between HAWS-B and HAWS-R of 10.7% and 11.2%, respectively (Table 5).

While overall crystallinity declined after *Par*GT-modification, FTIR-ATR analysis showed increased short-range molecular order at the granule surface in the modified (HAS-R) samples except from AOB (Table 5). Although this seemed contradictory, results obtained by these two techniques do not necessarily show parallel changes, reflecting the hierarchical structure of the starch granule and the localized nature of enzymatic action and interaction with different structural levels. Starch granules are composed of growth rings, each made up of alternating amorphous and semi-crystalline (lamellar) layers. The lamellar structure refers to internal, organized arrays of amylopectin double helices (typically with 9–10 nm periodicity), contributing to long-range order. By contrast, the granule surface, is more exposed, hydrated, and often amorphous, reflecting short-range organisation (~2 μm) (Bertoft, 2017; Bertoft et al., 2024). The FTIR-ATR and WAXS results suggested that *Par*GT modification disrupts long-range packing of double helices while simultaneously promoting their local reorganization on the surface (~2 μm penetration depth), catalysing the elongation of glucan chains which readily reassociate into short-range ordered double helices on the surface during annealing.

However, the increase in local double helix content at the surface (short-range order) does not necessarily translate to better lamellar packing across the entire granule, in accordance with a previous study (Tian, Petersen, et al., 2024). Regarding crystalline polymorphs (Table 5), V-type structures are generally more prominent in AOB samples possibly due to interactions with linear chains formed during modification. B-type crystallinity was higher in HPPS samples, consistent with the botanical origin (Tian, Liu, et al., 2024; Tian, Petersen, et al., 2024). A-type crystallinity was only detected in HAWS and remained low across all treatments, further highlighting its unique structural features.

3.4.6. HAS granules morphology and surface structure

The morphology of the HAS-N included the small, diverse AE-N granules, some of which exhibiting surface protrusions and elongated shapes (Fig. 5A), the lumpy AOB-N (Fig. 5D), the disc-like, round or C-shaped HAWS-N (Fig. 5G), and the large, oval and smooth granules characteristic of HPPS-N (Fig. 5J). Annealing at 75 °C (HAS-B samples) resulted in aggregation and loss of original granular morphology for HAWS (Fig. 5H) and HPPS (Fig. 5K), whereas AOB-B (Fig. 5E) and AE-B (Fig. 5B) did not undergo similar changes, consistent with their previously reported gelatinization onset temperatures of 87.8 °C and 83.6 °C, respectively (Tian, Liu, et al., 2024). The *Par*GT treated granules (HAS-R samples) occasional showed small holes on the surface as of AE-R (Fig. 5C, white arrow), possibly due to structural rearrangements of enzymatically modified surface chains. Notably, HPPS-R retained a smooth surface with minor defects (Fig. 5L, white arrows) maybe caused by milling during sample preparation. HAWS-R (Fig. 5I) also had small defects. Comparison of HAS-B and HAS-R granules revealed that *Par*GT modification did not visibly alter the surface of HAS-R, except possibly for AE-R (Fig. 5). This aligns with increasing FTIR ratios indicating higher surface crystallinity, expected to maintain surface smoothness.

3.5. Digestibility of granular HASs before and after modification

To date, only a single study (Jiang et al., 2014) has reported resistant starch (RS) formation through the action of thermophilic 4αGTs on starch, and none has evaluated RS content in thermophilic 4αGT-

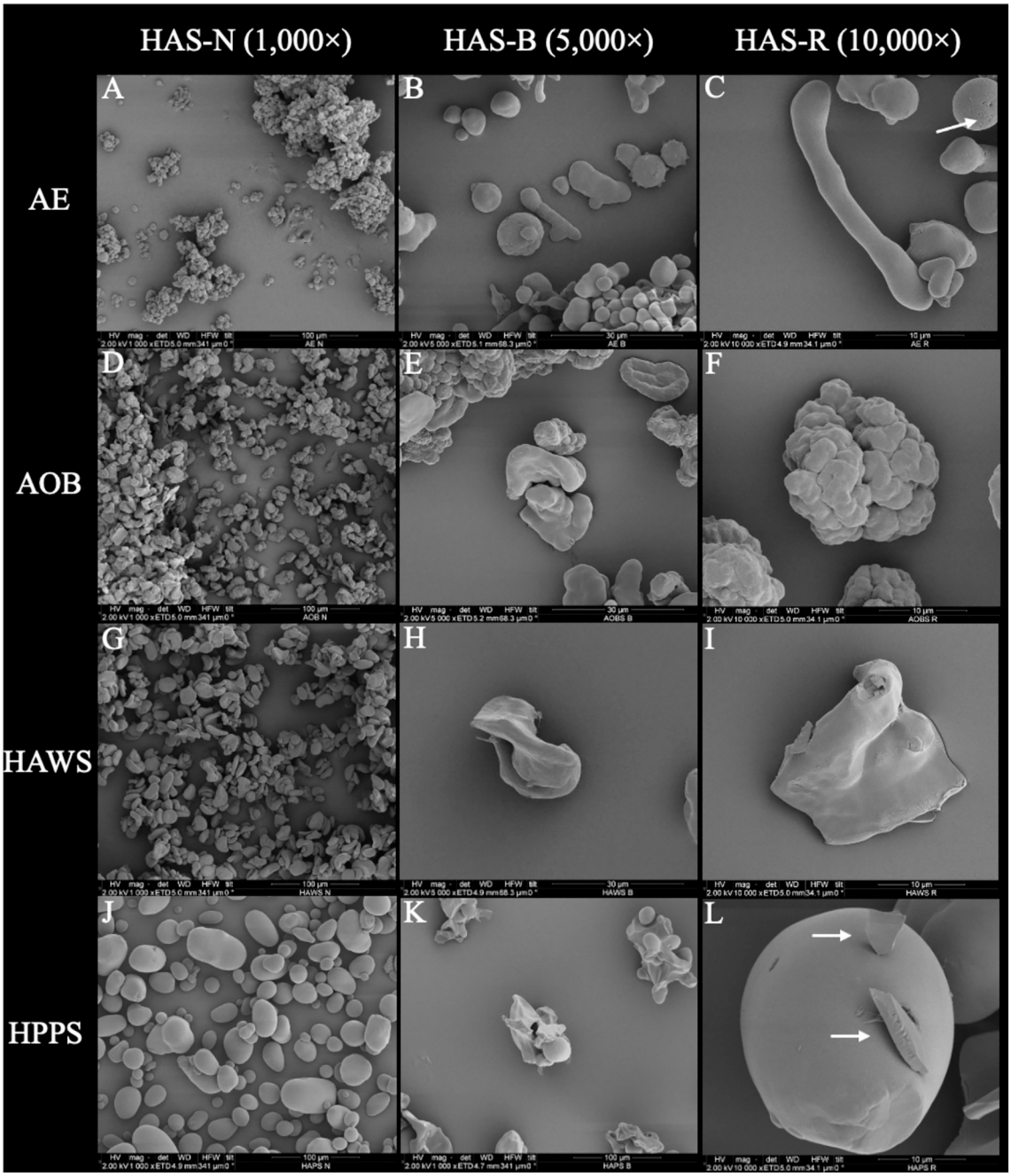

Fig. 5. HAS granules morphology and surface structure. (A) AE-N, (B) AE-B, (C) AE-R, (D) AOB-N, (E) AOB-B, (F) AOB-R, (G) HAWS-N, (H) HAWS-B, (I) HAWS-R, (J) HPPS-N, (K) HPPS-B, and (L) HPPS-R. HAS-N is depicted in 1000× magnification, while HAS-B and HAS-R are shown in 5000× and 10,000× magnification, respectively. For sample abbreviations see Table 1 and Section 2.8.

modified starch granules. Therefore, to evaluate the impact of the *Par*GT treatment, the HAS granules were subjected to the Englyst *in vitro* digestion procedure to investigate how structural changes translated into altered digestibility by glucoamylase (GA) and porcine pancreatic α-amylase (PPA), mimicking hydrolytic enzymes of the human gastrointestinal tract (Englyst et al., 1992). The digestibility was assessed from the amount of starch remaining after 3 h (C180), degradation rate constant (*k*), as well as the relative proportions of rapidly digested starch (RDS), slowly digested starch (SDS), and starch resistant to digestion (RS) (Fig. 6, Table S1). Overall, except for AOB-B, the percentage of digested starch (C180) increased most after heat treatment alone (B), compared to the native (N) and *Par*GT-treated (R) granules. Thus, C180 raised from 22.1% in HPPS-N to 59.3% in HPPS-B and from 66.9% in HAWS-N to 76.9% in HAWS-B (Table S1). The degradation rate constant *k* varied across treatments and HAS types (Table S1). In general, *k* increased by thermal modification (HAS-B compared to HAS-N samples) indicating larger accessibility to GA and PPA after heating. However, reaction by *Par*GT resulted in highest *k* values in the HAS-R compared to HAS—B, except for AOB-R. By contrast, lower *k* in AOB-R, compared to AOB-B, indicated that *Par*GT-induced structural changes, which slowed hydrolysis by GA and PPA. This was accompanied by 10-fold increase in SDS content, from 2.1% in AOB-B to 26.3% in AOB-R (Table S1), probably due to the increased relative crystallinity (Table 5). Heat-treatment (HAS-B samples) generally enhanced RDS and reduced RS compared to HAS-N samples, except for the RS of AOB-B (45.1%) and AOB-N (38.6%), indicating increased enzymatic resistance only in the heat-treated AOB (Table S1).

In contrast, effects of *Par*GT-treatment (HAS-R samples) were more variable. SDS increased and RS was reduced in AOB-R and AE-R compared to AOB-B and AE-B (Fig. 6, Table S1), suggesting that *Par*GT elicited remodelling of crystalline regions facilitating reaction by GA and PPA on those types of HAS (Tian et al., 2025). However, HPPS-R and HAWS-R had the highest RS contents, reaching 60% and 59%, respectively (Fig. 6, Table S1). This corresponded to 18% increase in RS content for HPPS-R compared to HPPS-B, while HAWS-R displayed 35% increase of RS relative to HAWS-B. Overall, the results underscore the starch-specific impact of *Par*GT-treatment on the *in vitro* digestion. Although higher crystallinity is generally associated with increased RS, RS is not determined solely by long-range order (Dhital et al., 2017). In the present work, despite the decrease in long-range crystallinity after *Par*GT treatment determined by WAXS, the increase in surface short-range order, as deduced from FTIR, resulted in higher RS content. This suggests that *Par*GT-driven chain reorganization alters helix packing in the lamellar layer while promoting surface localized ordered structures that favour RS formation, hindering the action of starch digestive enzymes. Comparatively, Jiang et al. (2014) reported an increase in RS from ~10.5% to ~17.6% after *Acidothermus cellulolyticus* 4αGT modification of gelatinised corn starch, highlighting this enzyme's moderate potential in changing digestibility. However, RS studies on granular starches remain scarce. Oh et al. (2008) examined *Thermotoga maritima* 4αGT acting on granular corn starch at 65 °C without inducing gelatinisation and observed changes in molecular weight and chain-length distribution, but RS was not quantified. Likewise, *Thermus aquaticus* 4αGT reacting on rice starch slurry at 75 °C mainly produced cyclodextrins (DP 5–19), and RS was not determined (Cho et al., 2009). In this context, the present work offers the first systematic evaluations of RS formation in *Par*GT-modified high-amylose starch granules under high-temperature, non-gelatinising conditions.

3.6. Interfacial kinetics of HAS hydrolysis by GA

To further describe the mechanism behind the *in vitro* resistance of the different granular HASs, the kinetics was analysed of the interfacial hydrolysis catalysed by GA. This involved combining conventional Michaelis-Menten (MM) kinetics for substrate in excess, with inverse MM-kinetics, where the enzyme is in excess, and *Langmuir* adsorption analysis to extract the interfacial kinetics parameters as well as the densities of GA attack- and binding-sites on the granular substrates.

The GA affinity ($1/K_d$) and binding capacity ($^{ads}\Gamma_{max}$, referred to as density of enzyme binding sites) obtained from *Langmuir* isotherms varied up to 12- and 10-fold, respectively, for the HASs granules (Table 6, Fig. S12). Comparison of $^{ads}\Gamma_{max}$ for HAS—N, —B and -R further indicated that GA recognized 1.4-fold fewer binding sites on AOB-B than AOB-N, consistent with the increase of RS in AOB-B (Fig. 6), whereas more GA binding sites were found on the other HAS-B than on the corresponding HAS-N samples. Thus, $^{ads}\Gamma_{max}$ was 2.1-fold higher on AE-B than AE-N (Table 6), in accordance with the decreased RS and concomitant increase in RDS contents in AE-B (Fig. 6).

In the interfacial catalysis for GA, the lowered density of attack sites ($^{kin}\Gamma_{max}$) indicated enhanced resistance of the starch granules to the enzymatic degradation (Tian et al., 2025; Wang, Tian, et al., 2024). Here, $^{kin}\Gamma_{max}$ values (Table 6) showed a weak albeit consistent correlation with the *in vitro* digestion parameters, C180, *k*, and RDS, SDS, and RS (Table S1). Thus, $^{kin}\Gamma_{max}$ was well correlated with the *in vitro* digestion parameter C180 corresponding to the starch degraded by GA and PPA after 180 min (Fig. 7C,F,I,L). Notably, the *Par*GT-modification of HPPS and HAWS reduced the density of GA attack sites, $^{kin}\Gamma_{max}$, for HAWS from 17.4 to 6.0 and HPPS from 2.1 to 1.4 nmol/g (Table 6), which also led to increased content of RS not degraded by *in vitro* digestion using GA and PPA, of 34% and 18%, respectively (Table S1).

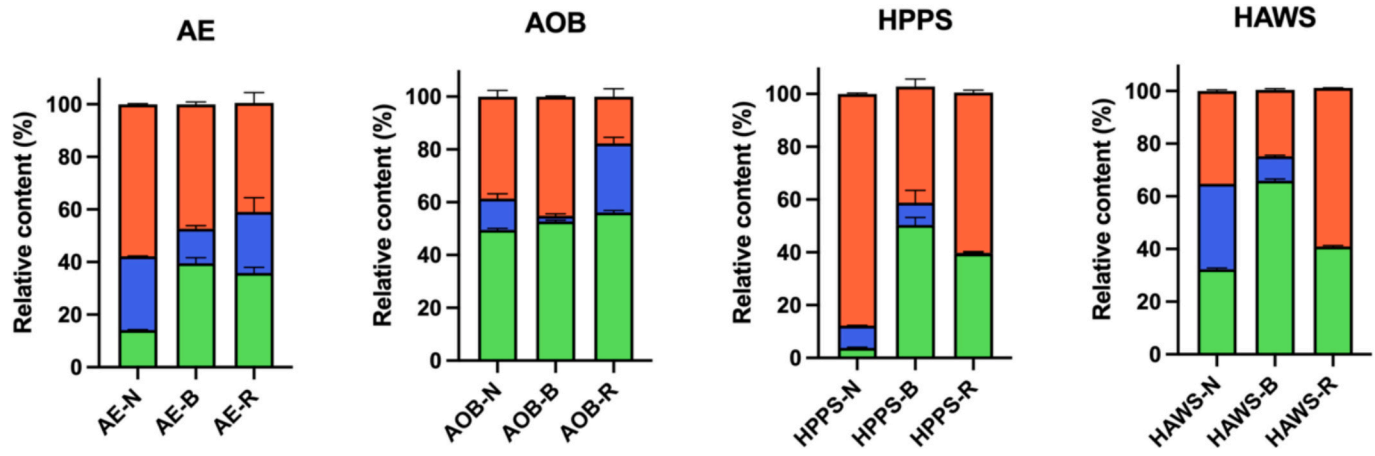

Fig. 6. Starch *in vitro* digestion. Contents of rapidly digested starch (RDS, green), slowly digested starch (SDS, blue) and resistant starch (RS, red). RDS refers to the fraction of starch digested within 20 min; SDS to the fraction digested between 20 and 120 min; and RS to the undigested starch remaining after 120 min. For sample abbreviations see Table 1 and Section 2.8.

Table 6
Interfacial kinetic and *Langmuir* adsorption parameters of GA reacting on HASs.

Starch[1]	k_{cat} (s^{-1})	$K_{1/2}$ ($g{\cdot}L^{-1}$)	$^{inv}k_{cat}$ ($nmol{\cdot}g^{-1}{\cdot}s^{-1}$)	$^{kin}\Gamma_{max}$ (nmol/g)	$^{ads}\Gamma_{max}$ (nmol/g)	A/B ratio	K_d (nM)
AE-N	220 ± 20 [c2]	35 ± 2 [a]	480 ± 30 [c]	2.2 ± 0.1 [c]	18 ± 1 [c]	11.8 ± 0.3 [a]	890 ± 105 [b]
AE-B	300 ± 15 [b]	20 ± 1 [b]	710 ± 20 [b]	2.4 ± 0.0 [b]	39 ± 4 [b]	6.1 ± 0.4 [b]	710 ± 100 [b]
AE-R	370 ± 20 [a]	10 ± 1 [c]	1020 ± 70 [a]	3.3 ± 0.0 [a]	62 ± 13 [a]	5.4 ± 0.9 [b]	1220 ± 130 [a]
AOB-N	150 ± 10 [b]	45 ± 3 [a]	1150 ± 100 [b]	1.5 ± 0.5 [a]	35 ± 7 [b]	9.2 ± 0.5 [a]	1140 ± 190 [a]
AOB-B	105 ± 7 [c]	30 ± 2 [b]	660 ± 75 [c]	1.3 ± 0.2 [a]	25 ± 0.5 [b]	5.0 ± 0.7 [b]	600 ± 6 [b]
AOB-R	170 ± 6 [a]	45 ± 6 [a]	1670 ± 100 [a]	2.0 ± 0.2 [a]	60 ± 8 [a]	3.2 ± 0.1 [c]	1220 ± 130 [a]
HAWS-N	130 ± 6 [b]	20 ± 1 [b]	1060 ± 80 [b]	8.3 ± 0.6 [b]	65 ± 2 [b]	12.7 ± 1.2 [b]	1710 ± 120 [b]
HAWS-B	230 ± 10 [a]	45 ± 5 [a]	3970 ± 150 [a]	17.4 ± 1.1 [a]	103 ± 2 [a]	17.0 ± 1.5 [b]	3400 ± 230 [a]
HAWS-R	65 ± 4 [c]	8 ± 1 [c]	430 ± 65 [c]	6.9 ± 0.5 [b]	29 ± 2 [c]	23.8 ± 2.9 [a]	290 ± 30 [c]
HPPS-N	70 ± 7 [c]	45 ± 4 [a]	60 ± 8 [c]	1.0 ± 0.2 [b]	15 ± 1.5 [c]	6.5 ± 0.5 [a]	550 ± 90 [b]
HPPS-B	270 ± 15 [a]	25 ± 3 [b]	580 ± 35 [a]	2.1 ± 0.3 [a]	31 ± 0.5 [b]	6.8 ± 0.3 [a]	950 ± 90 [a]
HPPS-R	165 ± 10 [b]	15 ± 1 [c]	230 ± 30 [b]	1.4 ± 0.1 [b]	45 ± 7 [a]	3.1 ± 0.3 [b]	1140 ± 75 [a]

[1] For sample abbreviations see Table 1 and Section 2.8.
[2] Values with different letters within the three types of the same HAS in the same column are significantly different at $p < 0.05$.

Thus, while GA still bound to the granules, with $^{ads}\Gamma_{max}$ values of 29 and 45 nmol/g for HAWS and HPPS, respectively (Table 6), fewer productive binding events occurred, substantially lowering catalytic turnover and increasing resistance to digestion. Accordingly, C180 decreased, in agreement with the enhanced resistance of these modified starches to GA (Fig. 7I,L).

The influence of crystallinity on the *in vitro* digestion resistance of starch granules was extensively investigated in the present study. Intriguingly, $^{kin}\Gamma_{max}$ and $^{ads}\Gamma_{max}$ correlated significantly with crystallinity, indicating the impact of crystallinity on resistance of starch granules through the ability of GA to recognise fewer attack and binding sites (Fig. S13).

4. Conclusion

This study demonstrates the potential of metagenomic environments as valuable reservoirs for the discovery of useful thermophilic CAZymes. Here, using the thermophilic 4-α-glucanotransferase *Par*GT from *Pyrobaculum arsenaticum*, modification of high-amylose granular starches was carried out at 75 °C under annealing-like conditions, leveraging their inherent high gelatinization temperatures. Rather than a uniform effect, *Par*GT induced distinct, HAS-type dependent structural and functional changes. Notably, RS contents increased in potato and wheat HAS, but neither in amylose-only barley nor amylose extender maize starch granules. This diverse behaviour of the *Par*GT modified HAS granules mirrored their different structural organisation and underscores how starch architecture critically influences enzymatic effects. For scale-up and application, practical aspects, like the 24 h reaction at sub-gelatinisation temperature, may need optimisation to ensure uniform heat and moisture distribution. These are manageable considerations that point to opportunities for process refinements including the exploration of other starch sources and hyperthermophilic enzymes to develop new functional starch-based materials. Overall, this study demonstrated that *Par*GT holds strong potential for selective starch modification, combining enzymatic and physical treatments to generate tailored biotechnological products. The results encourage future use in functional foods aimed at digestive health and glycaemic modulation as well as in controlled-release matrices, encapsulation of bioactive compounds, and sustainable starch-based biomaterials.

Abbreviations

4αGT	4-α-glucanotransferase
A/B ratio	Density of attack sites/density of binding sites ratio
AE	High-amylose maize starch AE 35
AM	Amylose
AOB	Amylose-only barley starch
AP	Amylopectin
B	Blank
BSA	Bovine serum albumin
CAZy	Carbohydrate-Active enzymes database
C180	Total amount of starch digested at 2 h
CAZymes	Carbohydrate active enzymes
CLD	Chain length distribution
CV	Column volume
D	Debranched
DP	Degree of polymerization
DSF	Differential scanning fluorimetry
E_{free}	Enzyme concentration in solution
FTIR-ATR	Fourier transform infrared-attenuated total reflectance
G3	Maltotriose
G4	Maltotetraose
G5	Maltopentaose
G6	Maltohexaose
G7	Maltoheptaose
GA	Glucoamylase
GH	Glycoside hydrolase
HAWS	High-amylose wheat starch
HAS	High-amylose starch
HPPS	High-amylose/high-phosphate potato starch
HPAEC-PAD	High-performance anion-exchange chromatography with pulsed amperometric detection
IPTG	Isopropyl-β-D-thiogalactopyranoside
k	Digestion velocity
K_d	Dissociation constant
LB	Luria-bertani
MM	Michaelis-menten
MOS	Maltooligosaccharides
N	Native
OD_{600}	Optical density at 600 nm
PPA	Porcine pancreas α-amylase
pI	Isoelectric point
R	Reaction
RDS	Rapidly digested starch
RS	Resistant starch
SDS	Slowly digested starch
SEC-RI	Size exclusion chromatography–refractive index detector
W	Whole
WAXS	Wide-angle X-ray scattering
$^{ads}\Gamma_{max}$	Density of binding sites
$^{kin}\Gamma_{max}$	Attack site density

CRediT authorship contribution statement

Oriana Sacco: Writing – review & editing, Writing – original draft, Software, Methodology, Investigation, Formal analysis. **Emilie Louise**

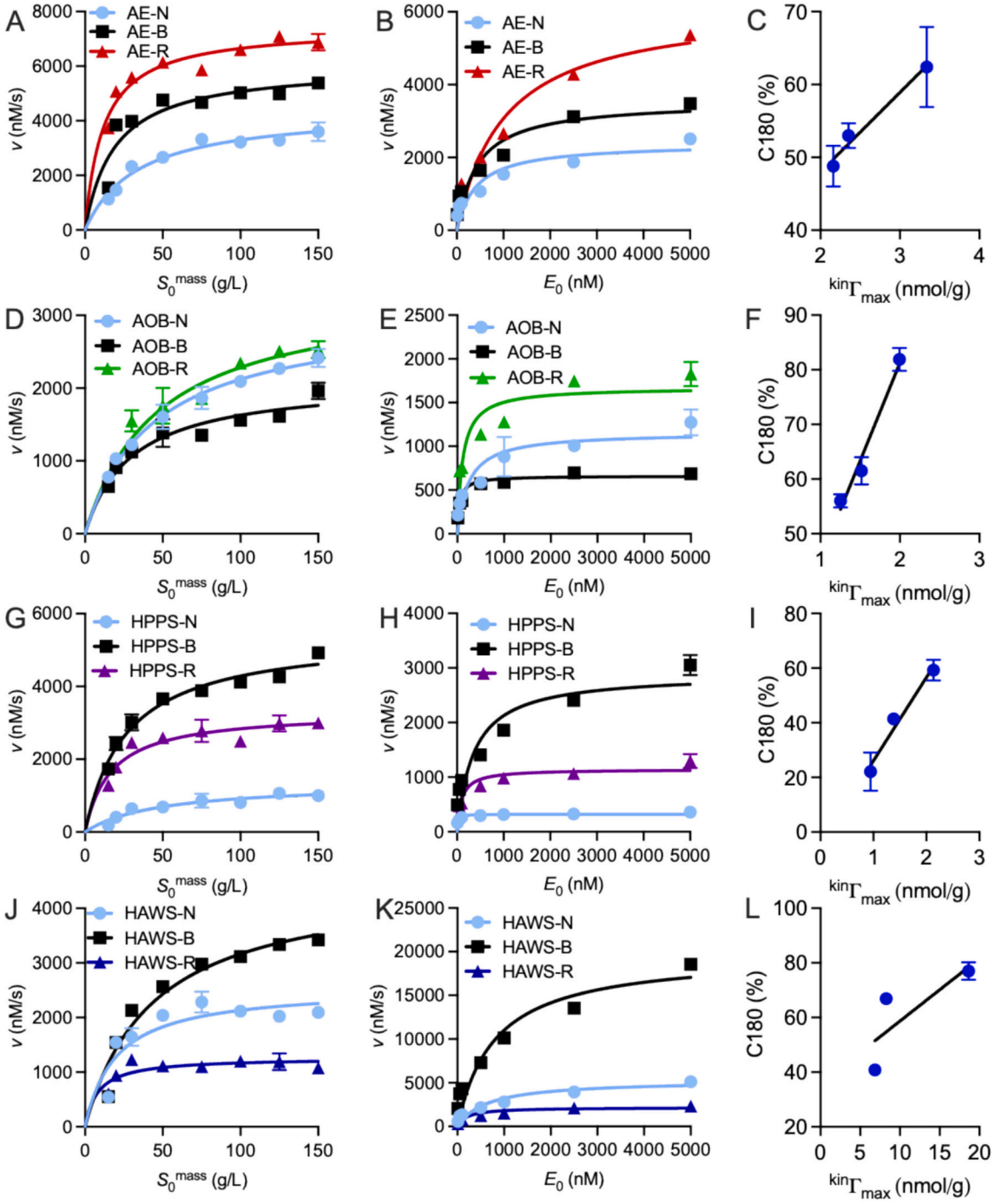

Fig. 7. Interfacial kinetics for GA reacting on HAS granules. Conventional MM-kinetics: (A) AOB, (D) AE, (G) HPPS, (J) HAWS. Inverse MM-kinetics: (B) AOB, (E) AE, (H) HPPS, (K) HAWS. Correlation analysis between C180 and $^{kin}\Gamma_{max}$ for (C) AOB, (F) AE, (I) HPPS, (L) HAWS. For sample abbreviations, see Table 1 and Section 2.8.

Johansen: Writing – review & editing, Software, Methodology. **Yu Tian:** Writing – review & editing, Supervision, Software, Methodology. **Jesper Holck:** Writing – review & editing, Methodology. **Jacob Judas Kain Kirkensgaard:** Writing – review & editing, Methodology. **Andreas Blennow:** Writing – review & editing, Supervision. **Federica De Lise:** Writing – review & editing. **Ali Shaikh-Ibrahim:** Writing – review & editing. **Marco Moracci:** Writing – review & editing, Supervision, Funding acquisition. **Nicola Curci:** Writing – review & editing, Supervision, Software, Methodology, Investigation, Conceptualization. **Birte Svensson:** Writing – review & editing, Supervision, Resources, Funding acquisition, Conceptualization. **Beatrice Cobucci-Ponzano:** Writing – review & editing, Supervision, Resources, Funding acquisition, Conceptualization. **Yu Wang:** Writing – review & editing, Writing – original draft, Supervision, Software, Methodology, Investigation, Formal analysis, Conceptualization.

Declaration of competing interest

The authors declare that they have no competing interests.

Acknowledgements

This work was supported by EU—Next Generation EU PNRR- Mission 4 "Education and Research"—Component 2 "From research to

business". Project IR0000032—ITINERIS, Italian Integrated Environmental Research Infrastructures System (CUP B53C22002150006), Ministry of University and Research- project NUTRAGE FOE-2021 DBA. AD005.225, and Independent Research Fund Denmark (FTP), project BioMarch, grant #3105-00327B (BS, AB). OS, FDL, ASI, MM, NC, and BCP belong to the European Research Infrastructure IBISBA-EU (www.ibisba.eu). Data were generated by accessing research infrastructure of the University of Copenhagen, including FOODHAY (Food and Health Open Innovation Laboratory, Danish Roadmap for Research Infrastructure). We thank Professor Alexander Büll for allowing us to use the Prometheus Panta for nano differential scanning fluorimetry (DSF) experiments. We are grateful to Antonio Suppa and Marco Petruzziello (CNR-IBBR) for administrative and technical assistance.

Appendix A. Supplementary data

Supplementary data to this article can be found online at https://doi.org/10.1016/j.carbpol.2026.124919.

Data availability

Data will be made available on request.

References

Abramson, J., Adler, J., Dunger, J., Evans, R., Green, T., Pritzel, A., … Jumper, J. M. (2024). Accurate structure prediction of biomolecular interactions with AlphaFold 3. *Nature, 630*(8016), 493–500. https://doi.org/10.1038/s41586-024-07487-w

Alarico, S., da Costa, M. S., & Empadinhas, N. (2008). Molecular and physiological role of the trehalose-hydrolyzing α-glucosidase from *Thermus thermophilus* HB27. *Journal of Bacteriology, 190*(7), 2298–2305. https://doi.org/10.1128/JB.01794-07

Arruda, T. R., Machado, G.d. O., Marques, C. S., Souza, A. L.d., Pelissari, F. M., Oliveira, T. V.d., & Silva, R. R. A. (2025). An overview of starch-based materials for sustainable food packaging: Recent advances, limitations, and perspectives. *Macromol, 5*(2), 19. https://doi.org/10.3390/macromol5020019

Ashraf, S., Siddiqui, M. A., Nisa, K., Ali, S., & Rashid, N. (2022). Gene cloning and characterization of Pcal_0222, α-amylase from *Pyrobaculum calidifontis*. *Pakistan Journal of Zoology, 54*(3), 537–542. https://doi.org/10.17582/journal.pjz/20200917190928

Ayoub, A. S., & Rizvi, S. S. (2009). An overview on the technology of cross-linking of starch for nonfood applications. *Journal of Plastic Film & Sheeting, 25*(1), 25–45.

Baghurst, P. A., Baghurst, K. I., & Record, S. J. (1996). Dietary fibre, non-starch polysaccharides and resistant starch: A review. *Food Australia, 48*, S3–S35.

Bertoft, E. (2017). Understanding starch structure: Recent progress. *Agronomy, 7*, 56. https://doi.org/10.3390/agronomy7030056

Bertoft, E., Blennow, A., & Hamaker, B. R. (2024). Perspectives on starch structure, function, and synthesis in relation to the backbone model of amylopectin. *Biomacromolecules, 25*(9), 5389–5401. https://doi.org/10.1021/acs.biomac.4c00369

Bhuiyan, S. H., Kitaoka, M., & Hayashi, K. (2003). A cycloamylose-forming hyperthermostable 4-α-glucanotransferase of *Aquifex aeolicus* expressed in *Escherichia coli*. *Journal of Molecular Catalysis B: Enzymatic, 22*, 45–53. https://doi.org/10.1016/S1381-1177(03)00005-5

Blennow, A., Wischmann, B., Houborg, K., Ahmt, T., Jørgensen, K., Engelsen, S. B., … Poulsen, P. (2005). Structure function relationships of transgenic starches with engineered phosphate substitution and starch branching. *International Journal of Biological Macromolecules, 36*(3), 159–168. https://doi.org/10.1016/j.ijbiomac.2005.05.006

Bradford, M. M. (1976). A rapid and sensitive method for the quantitation of microgram quantities of protein utilizing the principle of protein-dye binding. *Analytical Biochemistry, 72*, 248–254. https://doi.org/10.1006/abio.1976.9999

Brückner, S. (2000). Pulwin: A program for analyzing powder x-ray diffraction patterns. *Powder Diffraction, 15*, 218–219. https://doi.org/10.1017/S0885715600011118

Capron, I., Robert, P., Colonna, P., Brogly, M., & Planchot, V. (2007). Starch in rubbery and glassy states by FTIR spectroscopy. *Carbohydrate Polymers, 68*(2), 249–259. https://doi.org/10.1016/j.carbpol.2006.12.015

Carciofi, M., Blennow, A., Jensen, S. L., Shaik, S. S., Henriksen, A., Buléon, A., … Hebelstrup, K. H. (2012). Concerted suppression of all starch branching enzyme genes in barley produces amylose-only starch granules. *BMC Plant Biology, 12*, 223. https://doi.org/10.1186/1471-2229-12-223

Chen, P., Xu, R., Wang, J., Wu, Z., Yan, L., Zhao, W., Liu, Y., Ma, W., Shi, X., & Li, H. (2018). Starch biotransformation into isomaltooligosaccharides using thermostable alpha-glucosidase from *Geobacillus stearothermophilus*. *PeerJ, 6*, Article e5086. https://doi.org/10.7717/peerj.5086

Chen, S., Qiu, Z., Yang, Y., Wu, J., Jiao, W., Chen, Y., & Jin, C. (2024). Revisiting the evolution of multi-scale structures of starches with different crystalline structures during enzymatic digestion. *Foods (Basel, Switzerland), 13*(20), 3291. https://doi.org/10.3390/foods13203291

Chen, Y., McClements, D. J., Peng, X., Chen, L., Xu, Z., Meng, M., Ji, H., Long, J., Qiu, C., Zhao, J., & Jin, Z. (2023). Research progresses on enzymatic modification of starch with 4-α-glucanotransferase. *Trends in Food Science & Technology, 131*, 164–174. https://doi.org/10.1016/j.tifs.2022.11.025

Chen, Y., Wang, Y., Tian, Y., Svensson, B., & Blennow, A. (2024). Enzymatic synthesis of long-branched or short-branched starches with uniform molecular size. *Food Bioscience, 62*, Article 105353. https://doi.org/10.1016/j.fbio.2024.105353

Cho, K. H., Auh, J. H., Ryu, J. H., Kim, J. H., Park, K. H., Park, C. S., & Yoo, S. H. (2009). Structural modification and characterization of rice starch treated by Thermus aquaticus 4-α-glucanotransferase. *Food Hydrocolloids, 23*(8), 2403–2409. https://doi.org/10.1016/j.foodhyd.2009.06.019

Christensen, S. J., Madsen, M. S., Zinck, S. S., Hedberg, C., Sørensen, O. B., Svensson, B., & Meyer, A. S. (2024). Bioinformatics and functional selection of GH77 4-α-glucanotransferases for potato starch modification. *New Biotechnology, 79*, 39–49. https://doi.org/10.1016/j.nbt.2023.12.002

Chuang, S. C., Norat, T., Murphy, N., Olsen, A., Tjønneland, A., Overvad, K., … Vineis, P. (2012). Fiber intake and total and cause-specific mortality in the European prospective investigation into Cancer and nutrition cohort. *The American Journal of Clinical Nutrition, 96*(1), 164–174. https://doi.org/10.3945/ajcn.111.028415

Cifuente, J. O., Colleoni, C., Kalscheuer, R., & Guerin, M. E. (2024). Architecture, function, regulation, and evolution of α-glucans metabolic enzymes in prokaryotes. *Chemical Reviews, 124*(8), 4863–4934. https://doi.org/10.1021/acs.chemrev.3c00811

Compart, J., Singh, A., Fettke, J., & Apriyanto, A. (2023). Customizing starch properties: A review of starch modifications and their applications. *Polymers, 15*(16), 3491. https://doi.org/10.3390/polym15163491

Curci, N., Strazzulli, A., Iacono, R., De Lise, F., Maurelli, L., Di Fenza, M., … Moracci, M. (2021). Xyloglucan oligosaccharides hydrolysis by exo-acting glycoside hydrolases from hyperthermophilic microorganism *Saccharolobus solfataricus*. *International Journal of Molecular Sciences, 22*(7), 3325. https://doi.org/10.3390/ijms22073325

De Lise, F., Iacono, R., Moracci, M., Strazzulli, A., & Cobucci-Ponzano, B. (2023). Archaea as a model system for molecular biology and biotechnology. *Biomolecules, 13*(1), 114. https://doi.org/10.3390/biom13010114

Debet, M. R., & Gidley, M. J. (2006). Three classes of starch granule swelling: Influence of surface proteins and lipids. *Carbohydrate Polymers, 64*(3), 452–465. https://doi.org/10.1016/j.carbpol.2005.12.011

Demirkan, E., Mikami, B., Adachi, M., Higasa, T., & Utsumi, S. (2005). α-Amylase from *bacillus amyloliquefaciens*: Purification, characterization, raw starch degradation and expression in *E. Coli*. *Process Biochemistry, 40*(8), 2629–2636. https://doi.org/10.1016/j.procbio.2004.08.015

Dhital, S., Warren, F. J., Butterworth, P. J., Ellis, P. R., & Gidley, M. J. (2017). Mechanisms of starch digestion by α-amylase—Structural basis for kinetic properties. *Critical Reviews in Food Science and Nutrition, 57*(5), 875–892. https://doi.org/10.1080/10408398.2014.922043

Dobranowski, P. A., & Stintzi, A. (2021). Resistant starch, microbiome, and precision modulation. *Gut Microbes, 13*(1), Article 1926842. https://doi.org/10.1080/19490976.2021.1926842

Drula, E., Garron, M. L., Dogan, S., Lombard, V., Henrissat, B., & Terrapon, N. (2022). The carbohydrate-active enzyme database: Functions and literature. *Nucleic Acids Research, 50*(D1), D571–D577. https://doi.org/10.1093/nar/gkab1045

Englyst, H. N., Kingman, S. M., & Cummings, J. H. (1992). Classification and measurement of nutritionally important starch fractions. *European Journal of Clinical Nutrition, 46*, S33–S50.

Fonseca, L. M., Halal, S. L. M. E., Dias, A. R. G., & Zavareze, E. D. R. (2021). Physical modification of starch by heat-moisture treatment and annealing and their applications: A review. *Carbohydrate Polymers, 274*, Article 118665. https://doi.org/10.1016/j.carbpol.2021.118665

Gasteiger, E., Gattiker, A., Hoogland, C., Ivanyi, I., Appel, R. D., & Bairoch, A. (2003). ExPASy: The proteomics server for in-depth protein knowledge and analysis. *Nucleic Acids Research, 31*(13), 3784–3788. https://doi.org/10.1093/nar/gkg563

Gidley, M. J. (2013). Hydrocolloids in the digestive tract and related health implications. *Current Opinion in Colloid & Interface Science, 18*(4), 371–378. https://doi.org/10.1016/j.cocis.2013.04.003

Huber, R., Sacher, M., Vollmann, A., Huber, H., & Rose, D. (2000). Respiration of arsenate and selenate by hyperthermophilic archaea. *Systematic and Applied Microbiology, 23*(3), 305–314. https://doi.org/10.1016/S0723-2020(00)80058-2

Huggett, A. S., & Nixon, D. A. (1957). Use of glucose oxidase, peroxidase, and o-dianisidine in determination of blood and urinary glucose. *The Lancet, 273*, 368–370. https://doi.org/10.1016/S0140-6736(57)92595-3

Jacobs, H., & Delcour, J. A. (1998). Hydrothermal modifications of granular starch, with retention of the granular structure: A review. *Journal of Agricultural and Food Chemistry, 46*, 2895–2905. https://doi.org/10.1021/jf980169k

Jayakody, L., & Hoover, R. (2008). Effect of annealing on the molecular structure and physicochemical properties of starches from different botanical origins–A review. *Carbohydrate Polymers, 74*(3), 691–703. https://doi.org/10.1016/j.carbpol.2008.04.032

Ji, X., Wang, Z., Jin, X., Qian, Z., Qin, L., Guo, X., Yin, M., & Liu, Y. (2022). Effect of inulin on the pasting and retrogradation characteristics of three different crystalline starches and their interaction mechanism. *Frontiers in Nutrition, 9*, Article 978900. https://doi.org/10.3389/fnut.2022.978900

Jiang, H., Miao, M., Ye, F., Jiang, B., & Zhang, T. (2014). Enzymatic modification of corn starch with 4-α-glucanotransferase results in increasing slow digestible and resistant starch. *International Journal of Biological Macromolecules, 65*, 208–214. https://doi.org/10.1016/j.ijbiomac.2014.01.044

Jung, J. H., Kim, Y. J., Yang, S. K., Jeong, S., Holden, J. F., Seo, D. H., & Park, C. S. (2025). The Small Cycloamylose (CA15) synthesizing properties of 4-

α-glucanotransferase from hyperthermophilic *archaeon pyrobaculum arsenaticum* with its distinct disproportionation activity. *Journal of Agricultural and Food Chemistry, 73*(6), 3546–3558. https://doi.org/10.1021/acs.jafc.4c08064

Kamerling, J. P. (2007). Strategies for the structural analysis of carbohydrates. In J. P. Kamerling, G.-J. Boons, Y. C. Lee, A. Suzuki, N. Taniguchi, & A. G. J. Voragen (Eds.), *Vol. 2. Comprehensive Glycoscience: From chemistry to systems biology* (pp. 2/1–2/68). Elsevier. https://doi.org/10.1016/B978-044451967-2/00032-5.

Kaper, T., Talik, B., Ettema, T. J., Bos, H., van der Maarel, M. J., & Dijkhuizen, L. (2005). Amylomaltase of *Pyrobaculum aerophilum* IM2 produces thermoreversible starch gels. *Applied and Environmental Microbiology, 71*(9), 5098–5106. https://doi.org/10.1128/AEM.71.9.5098-5106.2005

Kari, J., Olsen, J. P., Jensen, K., Badino, S. F., Krogh, K. B. R. M., Borch, K., & Westh, P. (2018). Sabatier principle for interfacial (heterogeneous) enzyme catalysis. *ACS Catalysis, 8*(12), 11966–11972. https://doi.org/10.1021/acscatal.8b03547

Kim, J. E., Tran, P. L., Ko, J. M., Kim, S. R., Kim, J. H., & Park, J. T. (2021). Comparison of catalyzing properties of bacterial 4-α-glucanotransferases focusing on their cyclizing activity. *Journal of Microbiology and Biotechnology, 31*(1), 43–50. https://doi.org/10.4014/jmb.2009.09016

Leoni, C., Gattulli, B. A. R., Pesole, G., Ceci, L. R., & Volpicella, M. (2021). Amylomaltases in extremophilic microorganisms. *Biomolecules, 11*(9), Article 1335. https://doi.org/10.3390/biom11091335

Lever, M., Powell, J. C., Killip, M., & Small, C. W. (1973). A comparison of 4-hydroxybenzoic acid hydrazide (PAHBAH) with other reagents for the determination of glucose. *The Journal of Laboratory and Clinical Medicine, 82*(4), 649–655.

Li, H., Dhital, S., Flanagan, B. M., Mata, J., Gilbert, E. P., & Gidley, M. J. (2020). High-amylose wheat and maize starches have distinctly different granule organization and annealing behaviour: A key role for chain mobility. *Food Hydrocolloids, 105*, Article 105820. https://doi.org/10.1016/j.foodhyd.2020.105820

Li, H., Gidley, M. J., & Dhital, S. (2019). High-amylose starches to bridge the "fiber gap": Development, structure, and nutritional functionality. *Comprehensive Reviews in Food Science and Food Safety, 18*(2), 362–379. https://doi.org/10.1111/1541-4337.12416

Liu, D., Zhao, P., Chen, J., Yan, Y., & Wu, Z. (2022). Recent advances and applications in starch for intelligent active food packaging: A review. *Foods, 11*(18), 2879. https://doi.org/10.3390/foods11182879

Lombard, V., Henrissat, B., & Garron, M. L. (2025). CAZac: An activity descriptor for carbohydrate-active enzymes. *Nucleic Acids Research, 53*(D1), D625–D633. https://doi.org/10.1093/nar/gkae1045

Mehboob, S., Ahmad, N., Munir, S., Ali, R., Younas, H., & Rashid, N. (2020). Gene cloning, expression enhancement in Escherichia coli and biochemical characterization of a highly thermostable amylomaltase from *Pyrobaculum calidifontis*. *International Journal of Biological Macromolecules, 165*(Pt A), 645–653. https://doi.org/10.1016/j.ijbiomac.2020.09.071

Nakapong, S., Tumhom, S., Kaulpiboon, J., & Pongsawasdi, P. (2022). Heterologous expression of 4α-glucanotransferase: Overproduction and properties for industrial applications. *World Journal of Microbiology and Biotechnology, 38*(2), 36. https://doi.org/10.1007/s11274-021-03220-1

Oh, E. J., Choi, S. J., Lee, S. J., Kim, C. H., & Moon, T. W. (2008). Modification of granular corn starch with 4-α-glucanotransferase from *Thermotoga maritima*: Effects on structural and physical properties. *Journal of Food Science, 73*(3), C158–C166. https://doi.org/10.1111/j.1750-3841.2007.00655.x

Pandiselvam, R., Manikantan, M. R., Divya, V., Ashokkumar, C., Kaavya, R., Kothakota, A., & Ramesh, S. V. (2019). Ozone: An advanced oxidation technology for starch modification. *Ozone: Science & Engineering, 41*(6), 491–507.

Przylas, I., Tomoo, K., Terada, Y., Takaha, T., Fujii, K., Saenger, W., & Sträter, N. (2000). Crystal structure of amylomaltase from *Thermus aquaticus*, a glycosyltransferase catalysing the production of large cyclic glucans. *Journal of Molecular Biology, 296*(3), 873–886. https://doi.org/10.1006/jmbi.1999.3503

Punia Bangar, S., Ashogbon, A. O., Singh, A., Chaudhary, V., & Whiteside, W. S. (2022). Enzymatic modification of starch: A green approach for starch applications. *Carbohydrate Polymers, 287*, Article 119265. https://doi.org/10.1016/j.carbpol.2022.119265

Reddy Shetty, P., Batchu, U. R., Buddana, S. K., Sambasiva Rao, K., & Penna, S. (2021). A comprehensive review on α-D-glucans: Structural and functional diversity, derivatization and bioapplications. *Carbohydrate Research, 503*, Article 108297. https://doi.org/10.1016/j.carres.2021.108297

Robert, X., & Gouet, P. (2014). Deciphering key features in protein structures with the new ENDscript server. *Nucleic Acids Research, 42*(W1), W320–W324. https://doi.org/10.1093/nar/gku316

Schrödinger, L., & DeLano, W. (2020). PyMOL. Retrieved from http://www.pymol.org/pymol.

Seo, S. H., Choi, K. H., Hwang, S., Kim, J., Park, C. S., Rho, J. R., & Cha, J. (2011). Characterization of the catalytic and kinetic properties of a thermostable *Thermoplasma acidophilum* α-glucosidase and its transglucosylation reaction with arbutin. *Journal of Molecular Catalysis B: Enzymatic, 72*(3–4), 305–312. https://doi.org/10.1016/j.molcatb.2011.07.006

Sevenou, O., Hill, S. E., Farhat, I. A., & Mitchell, J. R. (2002). Organisation of the external region of the starch granule as determined by infrared spectroscopy. *International Journal of Biological Macromolecules, 31*(1–3), 79–85. https://doi.org/10.1016/s0141-8130(02)00067-3

Shaikh-Ibrahim, A., Curci, N., De Lise, F., Sacco, O., Di Fenza, M., Castaldi, S., … K. B. R., Moracci, M., & Cobucci-Ponzano, B.. (2025). Carbohydrate conversion in spent coffee grounds: Pretreatment strategies and novel enzymatic cocktail to produce value-added saccharides and prebiotic mannooligosaccharides. *Biotechnology for Biofuels and Bioproducts, 18*(1), 2. https://doi.org/10.1186/s13068-024-02601-6

Ślosarczyk, A., Klapiszewska, I., Skowrońska, D., Janczarek, M., Jesionowski, T., & Klapiszewski, Ł. (2023). A comprehensive review of building materials modified with metal and metal oxide nanoparticles against microbial multiplication and growth. *Chemical Engineering Journal, 466*, Article 143276. https://doi.org/10.1016/j.cej.2023.143276

Smith, A. M., & Zeeman, S. C. (2020). Starch: A flexible, adaptable carbon store coupled to plant growth. *Annual Review of Plant Biology, 71*, 217–245. https://doi.org/10.1146/annurev-arplant-050718-100241

Strazzulli, A., Cobucci-Ponzano, B., Iacono, R., Giglio, R., Maurelli, L., Curci, N., … Moracci, M. (2020). Discovery of hyperstable carbohydrate-active enzymes through metagenomics of extreme environments. *The FEBS Journal, 287*(6), 1116–1137. https://doi.org/10.1111/febs.15080

Thompson, J. D., Higgins, D. G., & Gibson, T. J. (1994). CLUSTAL W: Improving the sensitivity of progressive multiple sequence alignment through sequence weighting, position-specific gap penalties and weight matrix choice. *Nucleic Acids Research, 22*(22), 4673–4680. https://doi.org/10.1093/nar/22.22.4673

Tian, Y., Liu, X., Kirkensgaard, J. J. K., Khakimov, B., Enemark-Rasmussen, K., Hebelstrup, K. H., … Zhong, Y. (2024). Characterization of different high amylose starch granules. Part I: Multi-scale structures and relationships to thermal properties. *Food Hydrocolloids, 146*, Article 109286. https://doi.org/10.1016/j.foodhyd.2023.109286

Tian, Y., Petersen, B. L., Liu, X., Li, H., Kirkensgaard, J. J. K., Enemark-Rasmussen, K., … Blennow, A. (2024). Characterization of different high amylose starch granules. Part II: Structure evolution during digestion and distinct digestion mechanisms. *Food Hydrocolloids, 149*, Article 109593. https://doi.org/10.1016/j.foodhyd.2023.109593

Tian, Y., Wang, Y., Liu, X., Herburger, K., Westh, P., Møller, M. S., … Blennow, A. (2023). Interfacial enzyme kinetics reveals degradation mechanisms behind resistant starch. *Food Hydrocolloids, 140*, Article 108621. https://doi.org/10.1016/j.foodhyd.2023.108621

Tian, Y., Wang, Y., Liu, X., Westh, P., Møller, M. S., Hebelstrup, K. H., … Zhong, Y. (2025). Unravelling the mechanism of enzymatic resistance in different high amylose starch granules. *Carbohydrate Polymers, 368*, Article 124052. https://doi.org/10.1016/j.carbpol.2025.124052

Van der Maarel, M. J. E. C., Capron, I., Euverink, G. J. W., Bos, H. T., Kaper, T., Binnema, D. J., & Steeneken, P. A. M. (2005). A novel thermoreversible gelling product made by enzymatic modification of starch. *Starch-Stärke, 57*(10), 465–472. https://doi.org/10.1002/star.200500409

Wang, L., Liu, Q., Wu, X., Huang, Y., Wise, M. J., Liu, Z., & Wang, C. (2019). Bioinformatics analysis of metabolism pathways of archaeal energy reserves. *Scientific Reports, 9*(1), 1034. https://doi.org/10.1038/s41598-018-37768-0

Wang, S., & Copeland, L. (2015). Effect of acid hydrolysis on starch structure and functionality: A review. *Critical Reviews in Food Science and Nutrition, 55*(8), 1081–1097. DOI.

Wang, Y., Li, X., Ji, H., Zheng, D., Jin, Z., Bai, Y., & Svensson, B. (2020). Thermophilic 4-α-glucanotransferase from *Thermoproteus uzoniensis* retards the long-term retrogradation but maintains the short-term gelation strength of tapioca starch. *Journal of Agricultural and Food Chemistry, 68*(20), 5658–5667. https://doi.org/10.1021/acs.jafc.0c00927

Wang, Y., Pang, C., Mohammad-Beigi, H., Li, X., Wu, Y., Lin, M. K. T. H., … Svensson, B. (2024). Sequential starch modification by branching enzyme and 4-α-glucanotransferase improves retention of curcumin in starch-alginate beads. *Carbohydrate Polymers, 323*, Article 121387. https://doi.org/10.1016/j.carbpol.2023.121387

Wang, Y., Tian, Y., Christensen, S. J., Blennow, A., Svensson, B., & Møller, M. S. (2024). An enzymatic approach to quantify branching on the surface of starch granules by interfacial catalysis. *Food Hydrocolloids, 146*, Article 109162. https://doi.org/10.1016/j.foodhyd.2023.109162

Wang, Y., Tian, Y., Møller, M. S., Jin, Z., Li, X., & Svensson, B. (2025). Exploring the enzymatic landscape of 4-α-glucanotransferases in carbohydrate bioprocessing. *Biotechnology Advances, 86*, Article 108737. https://doi.org/10.1016/j.biotechadv.2025.108737

Wang, Y., Tian, Y., Rennison, A. P., Blennow, A., Westh, P., Svensson, B., & Møller, M. S. (2025). Applying the Sabatier principle to decipher the surface-structure-dependent catalysis of different starch granules by pullulanase. *Journal of the American Chemical Society Au, 5*(1), 55–60. https://doi.org/10.1021/jacsau.4c00932

Warren, F. J., Gidley, M. J., & Flanagan, B. M. (2016). Infrared spectroscopy as a tool to characterise starch ordered structure–a joint FTIR-ATR, NMR, XRD and DSC study. *Carbohydrate Polymers, 139*, 35–42. https://doi.org/10.1016/j.carbpol.2015.11.066

Wei, T., & Simko, V. (2017). R Package "Corrplot": Visualization of a correlation matrix (Version 0.84). https://github.com/taiyun/corrplot.

Yin, Z., Liu, X., Guo, L., Ren, M., Kang, W., Ma, C., & Sun-Waterhouse, D. (2023). The potential of dietary fiber in building immunity against gastrointestinal and respiratory disorders. *Critical Reviews in Food Science and Nutrition, 64*(33), 13318–13336. https://doi.org/10.1080/10408398.2023.2266462

Zhong, Y., Liu, L., Qu, J., Blennow, A., Hansen, A. R., Wu, Y., … Liu, X. (2020). Amylose content and specific fine structures affect lamellar structure and digestibility of maize starches. *Food Hydrocolloids, 108*, Article 105994. https://doi.org/10.1016/j.foodhyd.2020.105994

Zhong, Y., Qu, J. Z., Liu, X., Ding, L., Liu, Y., Bertoft, E., … Blennow, A. (2022). Different genetic strategies to generate high amylose starch mutants by engineering the starch biosynthetic pathways. *Carbohydrate Polymers, 287*, Article 119327. https://doi.org/10.1016/j.carbpol.2022.119327

Zhu, F. (2017). Encapsulation and delivery of food ingredients using starch based systems. *Food Chemistry, 229*, 542–552. https://doi.org/10.1016/j.foodchem.2017.02.101